Climate controlled root zone parameters show potential to improve water flux simulations by land surface models

Fransje van Oorschot[1,2], Ruud J. van der Ent[1], Markus Hrachowitz[1], and Andrea Alessandri[2,3]

[1]Department of Water Management, Faculty of Civil Engineering and Geosciences, Delft University of Technology, Delft, The Netherlands
[2]Royal Netherlands Meteorological Institute (KNMI), De Bilt, The Netherlands
[3]Institute of Atmospheric Sciences and Climate, National Research Council of Italy (CNR-ISAC), Bologna, Italy

Correspondence: Fransje van Oorschot (f.vanoorschot@tudelft.nl)

Abstract. The root zone storage capacity (S_r) is the maximum volume of water in the subsurface that can potentially be accessed by vegetation for transpiration. It influences the seasonality of transpiration as well as fast and slow runoff processes. Many studies have shown that S_r is heterogeneous as controlled by local climate conditions, which affect vegetation strategies in sizing their root system able to support plant growth and to prevent water shortages. Root zone parameterization in most land surface models does not account for this climate control on root development, being based on look-up tables that prescribe worldwide the same root zone parameters for each vegetation class. These look-up tables are obtained from measurements of rooting structure that are scarce and hardly representative of the ecosystem scale. The objective of this research is to quantify and evaluate the effects of a climate controlled representation of S_r on the water fluxes modeled by the HTESSEL land surface model. Climate controlled S_r is here estimated with the "memory method" (MM) in which S_r is derived from the vegetation's memory of past root zone water storage deficits. $S_{r,MM}$ is estimated for 15 river catchments over Australia across three contrasting climate regions: tropical, temperate and Mediterranean. Suitable representations of $S_{r,MM}$ are implemented in an improved version of HTESSEL (MD) by accordingly modifying the soil depths to obtain a model $S_{r,MD}$ that matches $S_{r,MM}$ in the 15 catchments. In the control version of HTESSEL (CTR), $S_{r,CTR}$ is larger than $S_{r,MM}$ in 14 out of 15 catchments. Furthermore, the variability among the individual catchments of $S_{r,MM}$ (117–722 mm) is considerably larger than of $S_{r,CTR}$ (491–725 mm). The climate controlled representation of S_r in the MD version results in a significant and consistent improvement of the modeled monthly seasonal climatology (1975–2010) and inter-annual anomalies of river discharge compared with observations. However, the effects on biases in long-term annual mean ~~fluxes~~ river discharge are small and mixed. The modeled monthly seasonal climatology of the catchment discharge improved in MD compared to CTR: the correlation with observations increased significantly from 0.84 to 0.90 in tropical catchments, from 0.74 to 0.86 in temperate catchments and from 0.86 to 0.96 in Mediterranean catchments. Correspondingly, the correlations of the inter-annual discharge anomalies improve significantly in MD from 0.74 to 0.78 in tropical catchments, from 0.80 to 0.85 in temperate catchments and from 0.71 to 0.79 in Mediterranean catchments. The results indicate that the use of climate controlled $S_{r,MM}$ can significantly improve the timing of modeled discharge and, by extension, also evaporation fluxes in land surface models. On the other hand, the method has not shown to significantly reduce long-term climatological model biases over the catchments considered for this study.

1 Introduction

Vegetation controls the partitioning of precipitation into evaporation and runoff by transporting water through their roots to the atmosphere and is thereby key in the representation of land surface-atmosphere interactions (Milly, 1994; Seneviratne et al., 2010). The moisture flow from the land surface to the atmosphere through vegetation root water uptake is defined as transpiration and is globally the largest water flux from terrestrial ecosystems (Schlesinger and Jasechko, 2014). The contribution of transpiration to total land evaporation is regulated by the interplay between the atmospheric water demand and the soil moisture within the reach of vegetation's roots. The root zone is defined as the part of the subsurface where vegetation has developed roots and can be characterized by parameters such as root depth and root density. The importance of the root zone in land surface and climate modelling is widely acknowledged and multiple studies emphasize the climate sensitivity to changes in the vegetation's root zone (Mahfouf et al., 1996; Desborough, 1997; Zeng et al., 1998; de Rosnay and Polcher, 1998; Norby and Jackson, 2000; Feddes et al., 2001; Teuling et al., 2006). However, the parameterization of the root zone in state-of-the-art land surface models (LSMs) is a possible cause for the large uncertainties in water flux representations in these models (Gharari et al., 2019), which is in particular true for land evaporation simulations (Pitman, 2003; Seneviratne et al., 2006; Wartenburger et al., 2018).

The hydrologically relevant magnitude of the vegetation's root zone can be described by the root zone water storage capacity S_r, that represents the maximum subsurface moisture volume that can be accessed by the vegetation's roots. The size of S_r controls the variability and timing of water fluxes and specifically the ability of vegetation to maintain transpiration during the dry season when there is little to no recharge (Milly, 1994). It is important to note that S_r is not necessarily proportional to the depth of roots. While root depth only describes the vertical root profile, S_r also accounts for lateral root extent as well as root density. For example, an ecosystem covered by deep rooting vegetation with roots with low density likely has a smaller S_r than one covered by vegetation with shallow, high density roots (Singh et al., 2020).

However, most global LSMs do not have the explicit objective to estimate S_r and rather aim for a description of root zone parameters (e.g. root depth, root density and root distribution) for different vegetation classes combined with soil type information and a model-dependent fixed soil depth. The generally shallow ($< 2\,\mathrm{m}$) (Pan et al., 2020) fixed soil depth limits the size of S_r and, as a consequence, also the moisture extraction by roots from deep soil layers (Kleidon and Heimann, 1998; Sakschewski et al., 2020). LSMs use look-up tables that prescribe worldwide the same root zone parameters for each combination of vegetation and soil class as obtained from a very limited number of point-scale observations of rooting structure (Canadell et al., 1996; Jackson et al., 1996; Zeng et al., 1998; Schenk and Jackson, 2002a, b). The spatial distribution of the root zone parameterization in LSMs is obtained by combining these look-up table values with maps of vegetation cover and soil texture. The limitations of this approach are as follows: the root observations are 1) uncertain due to the fact that they mostly vertically extrapolate root measurements while excavating only the first meter or less (Schenk and Jackson, 2002a, b), 2) do not adequately represent global distributions of root structures because observations are extremely scarce: e.g. the Schenk

and Jackson (2002b) dataset includes 475 root profiles in 209 geographical locations, 3) observations of individual plants that do not represent spatial variations in ecosystem composition at scales larger than the plot scale and 4) snapshots in time and, therefore, do not represent their evolution over time due to continuous adaptation of ecosystems to changing environmental conditions.

An alternative to the look-up tables based on point-scale root observations for describing the vegetation's root zone is a climate controlled approach. The only LSM to our knowledge in which climate controlled root zone parameters are used is the JSBACH3.2 model (Hagemann and Stacke, 2015) in which rooting depths are based on the optimisation model of net primary production from Kleidon (2004). Yet, there is general strong evidence that climate is the dominant control of root development in many environments, as vegetation tends to optimize its above- and below-ground carbon investment in order to optimally function by avoiding water shortages and maintaining transpiration and productivity (Collins and Bras, 2007; Guswa, 2008; Sivandran and Bras, 2013). For example, it is likely that trees in a dry climate develop a larger S_r than trees in a wet climate because trees in a dry climate need to invest more in growing roots to sustain their water demand (Gentine et al., 2012; Gao et al., 2014).

A widely applied climate controlled approach in catchment hydrological studies to describe S_r is the "memory method". In this method S_r is derived from water storage deficit calculations in the root zone at catchment scale, assuming vegetation is able to keep memory of past deficit conditions to size roots in such a way to guarantee continuous access to water (hereinafter $S_{r,MM}$) (Gentine et al., 2012; Gao et al., 2014). Recent studies demonstrated that this method provides plausible catchment-scale estimates of S_r (e.g., Gao et al., 2014; Nijzink et al., 2016; Wang-Erlandsson et al., 2016; Hrachowitz et al., 2020), that result in improvements in modelling catchment discharge compared to soil derived S_r estimates (De Boer-Euser et al., 2016). However, climate controlled root zone parameters have not yet been widely incorporated in LSMs.

The objective of this study is to quantify and evaluate the effects of a climate controlled representation of S_r on the water fluxes modeled by the HTESSEL land surface model. Specifically we will test the hypothesis that implementing $S_{r,MM}$ in HTESSEL can improve the modeled magnitude and timing of catchment discharge and evaporation fluxes. By applying the memory method for estimating ecosystem-scale S_r for use in LSMs, the first three limitations of using sparse root observations mentioned above can be overcome, but it should be acknowledged that, although the memory method in principle allows to adaptively update S_r, in this work we use a fixed value in time. In this study, $S_{r,MM}$ values representative for the 1973–2010 time period are estimated for 15 Australian catchments across different climate regions (Sect. 2.3 and Appendix A). The $S_{r,MM}$ estimates are then used to constrain the S_r in HTESSEL (Sect. 2.5). Section 3 evaluates the effects on discharge and evaporation in HTESSEL by performing offline simulations with and without the improved representation of S_r. Finally in Sect. 4 and 5 the potential for a wider application of climate controlled root zone parameters is discussed.

2 Methods

2.1 Study area

Australia is characterized by large spatial differences in precipitation (Fig. 1), vegetation coverage and temperatures, varying from hot and dry deserts in the interior to tropical forests with a monsoon season in the north. We have selected 15 Australian river catchments with station observations of river discharge at the outlet of the catchment to estimate S_r applying the memory method (Fig. 1; Table S1) (Australian Government Bureau of Meteorology, 2019). The catchments are selected based on available discharge data (at least 30 years of station observations), size (at least one third of the land surface model grid cell area of approximately 5500 km^2 in order to spatially extrapolate catchment characteristics to grid cells) and differences in climate (spatial spread of the catchments across Australia for the analysis of different climate zones). The catchments are classified in three climate regions based on their hydrological characteristics (Table 1; Fig. 2; Table S2). The tropical catchments are characterized by pronounced seasonality of rainfall with a seasonality index of precipitation (I_S) of 0.7 or higher, while temperate and Mediterranean catchments have year-round rainfall (I_S <0.7). The Mediterranean catchments are characterized by a time-lag ϕ between long-term mean maximum monthly potential evaporation E_p and precipitation P of five or six months, while in tropical and temperate catchments mean maximum monthly E_p and P occur within three months.

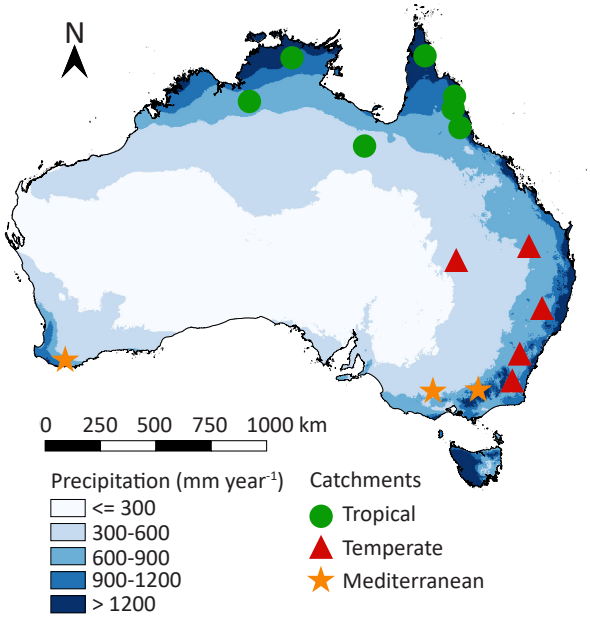

Figure 1. Location of the 15 study catchments within Australia. The green, red and orange markers indicate the climate region and the blue shades indicate long-term mean annual precipitation (Australian Government Bureau of Meteorology, 2019). A list of the catchments and their characteristics is provided in Table S1.

Table 1. Average hydrological characteristics of the catchments in the three climate regions for the time period 1973–2010 with long-term mean annual discharge $\overline{Q}$, precipitation $\overline{P}$ and potential evaporation $\overline{E_p}$, aridity index $I_A = \overline{E_p}/\overline{P}$, seasonality index of precipitation $I_S = \frac{1}{\overline{P_a}} \sum_{m=1}^{m=12} |\overline{P_m} - \frac{\overline{P_a}}{12}|$, with $\overline{P_a}$ the annual mean precipitation and $\overline{P_m}$ the monthly mean precipitation of month m (Gao et al., 2014) and the time-lag ϕ between long-term mean maximum monthly precipitation (P) and potential evaporation (E_p). Values for all individual catchments are provided in Table S2.

Climate region	$\overline{Q}$ (mm year^{-1})	$\overline{P}$ (mm year^{-1})	$\overline{E_p}$ (mm year^{-1})	I_A (-)	I_S (-)	ϕ (months)
Tropical (7 catchments)	302	1101	1869	2	0.9	2.3
Temperate (5 catchments)	57	651	1488	2.5	0.2	0.6
Mediterranean (3 catchments)	53	879	1276	1.7	0.3	5.7

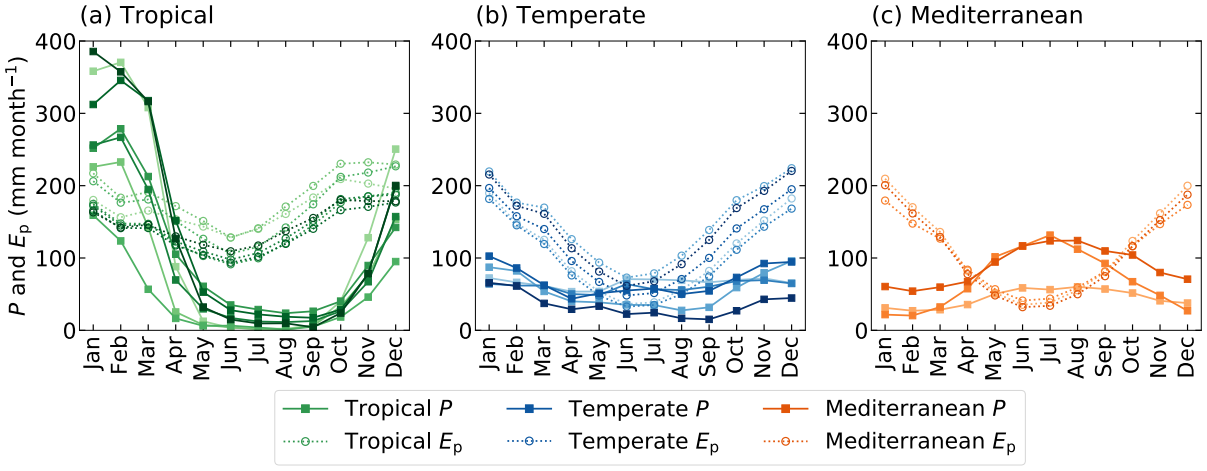

Figure 2. Monthly seasonal climatology of precipitation (P) and potential evaporation (E_p) for the (a) tropical, (b) temperate and (c) Mediterranean catchments with the solid lines P and the dashed lines E_p for the time series 1973–2010. The different shades indicate the 15 individual study catchments.

2.2 Data

For this study we use daily discharge data from station observations in the catchments for the time period 1973–2010 (Australian Government Bureau of Meteorology, 2019). For the same time period we use daily precipitation and daily mean temperature data from the GSWP-3 dataset on a regular 0.5°grid (Kim, 2017). Daily E_p is calculated applying the Hargreaves and Samani formulation, based on temperature and radiation (Hargreaves and Samani, 1982; Mines ParisTech Solar radiation Data, 2016). The FLUXCOM RS+METEO dataset is used as a reference dataset to benchmark modeled actual evaporation.

FLUXCOM provides a gridded product of interpolated monthly evaporation as a fusion of FLUXNET eddy covariance towers, satellite observations and meteorological data (GSWP-3) for the time period 1975–2010 (Jung et al., 2019). This dataset has shown plausible estimates of mean annual and seasonal evaporation and is generally considered as a suitable tool for global land model evaluations (Jung et al., 2019; Ma et al., 2020). However, we found considerable differences between the long-term annual mean evaporation $\overline{E}_{\text{FLUXCOM}}$ and $\overline{E}$ derived from the catchment water balance ($\overline{E}_{\text{WB}}$) based on observed Q and GSWP-3 P ($\overline{E}_{\text{WB}} = \overline{P} - \overline{Q}$) (Fig. 3). Figure 3 clearly illustrates that the $\overline{E}_{\text{FLUXCOM}}$ is consistently lower than $\overline{E}_{\text{WB}}$ with an average difference of $150\,\text{mm}\,\text{year}^{-1}$, equivalent to about 20 % of the long-term water balances. $\overline{E}_{\text{WB}}$ is likely to be more reliable than $\overline{E}_{\text{FLUXCOM}}$ because $\overline{E}_{\text{WB}}$ provides an integrated catchment scale estimate as it is derived from observations of Q assuming that the catchments are large enough to neglect deep groundwater drainage to or from other catchments (Bouaziz et al., 2018; Condon et al., 2020). In addition, $\overline{E}_{\text{FLUXCOM}}$ is based on point scale estimates of FLUXNET stations that do not coincide with and are mostly located far from the study catchments (Pastorello et al., 2020). The discrepancy between the FLUXCOM and the catchment water balance is addressed by scaling the monthly FLUXCOM evaporation:

$$E_{\text{FLUXCOM-WB}} = E_{\text{FLUXCOM}} \frac{\overline{E}_{\text{WB}}}{\overline{E}_{\text{FLUXCOM}}} \tag{1}$$

with $E_{\text{FLUXCOM-WB}}$ the monthly reference evaporation representative for the catchment scale, E_{FLUXCOM} from Jung et al. (2019) in the catchment corresponding grid cells and $\frac{\overline{E}_{\text{WB}}}{\overline{E}_{\text{FLUXCOM}}}$ the catchment specific scaling factor.

We use gridded data of vegetation type and coverage derived from the GLCC1.2 (ECMWF, 2016) and soil texture data from the FAO/UNESCO Digital Soil Map of the World (FAO, 2003). Characteristics of the different soil textures are based on the Van Genuchten soil parameters (Van Genuchten, 1980). These data are needed as input of the HTESSEL model and for the estimation of S_{r}.

2.3 Memory method for estimating root zone storage capacity

$S_{\text{r,MM}}$ is estimated based on catchment hydrometeorological data, according to the methodology described in the studies of De Boer-Euser et al. (2016), Nijzink et al. (2016) and Wang-Erlandsson et al. (2016). $S_{\text{r,MM}}$ is based on an extreme value analysis of the annual maximum water storage deficits in the vegetation's root zone (S_{d}). S_{d} maximizes during dry periods, and, therefore, S_{r} represents an upper limit of root zone storage assuming that vegetation has sufficient access to water to overcome these dry periods. The cumulative water storage deficit ~~(~~S_{d} (mm) in the root zone is based on daily time series of effective precipitation P_{e} ($\text{mm}\,\text{day}^{-1}$) and transpiration E_{t} ($\text{mm}\,\text{day}^{-1}$) for the time period ~~$t_0$ – t_1 of~~ 1973–2010 and is described by:

$$S_{\text{d}}(t) = \max(0, -\int_{t_0}^{t_1 \tau} (P_{\text{e}} - E_{\text{t}})\text{d}t) \tag{2}$$

~~where~~ with an integration from t_0 that corresponds to the first day in the hydrological year 1973 to τ that corresponds to the daily time steps ending at the last day of the hydrological year 2010. P_{e} ($\text{mm}\,\text{day}^{-1}$) is derived from the water balance of the interception storage S_{i}:

$$\frac{\text{d}S_{\text{i}}}{\text{d}t} = P - E_{\text{i}} - P_{\text{e}} \tag{3}$$

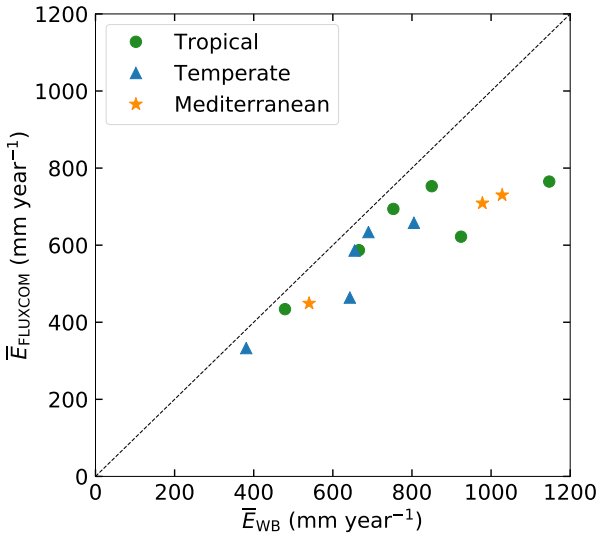

Figure 3. Long-term mean annual evaporation ($\overline{E}$) as estimated from long-term water balance data ($\overline{E}_{\mathrm{WB}}$) compared to the FLUXCOM dataset ($\overline{E}_{\mathrm{FLUXCOM}}$) for the 1975–2010 period.

with P the precipitation ($\mathrm{mm\,day^{-1}}$) and E_{i} the interception evaporation ($\mathrm{mm\,day^{-1}}$). Equation 3 is solved by the following relations:

$$E_{\mathrm{i}} P_{\mathrm{e}} = \begin{cases} 0 & \text{if } P\mathrm{d}t + S_{\mathrm{i}} \leq S_{\mathrm{i,max}} \\ \frac{P\mathrm{d}t + S_{\mathrm{i}} - S_{\mathrm{i,max}}}{\mathrm{d}t} & \text{if } P\mathrm{d}t + S_{\mathrm{i}} > S_{\mathrm{i,max}} \end{cases} \tag{4}$$

$$P_{\mathrm{e}} S_{\mathrm{i}}^{*} = S_{\mathrm{i}} - P_{\mathrm{e}}\mathrm{d}t \tag{5}$$

$$E_{\mathrm{i}} = \begin{cases} E_{\mathrm{p}} & \text{if } E_{\mathrm{p}}\mathrm{d}t < S_{\mathrm{i}}^{*} \\ \frac{S_{\mathrm{i}}^{*}}{\mathrm{d}t} & \text{if } E_{\mathrm{p}}\mathrm{d}t \geq S_{\mathrm{i}}^{*} \end{cases} \tag{6}$$

where E_{p} is the potential evaporation ($\mathrm{mm\,day^{-1}}$) and $S_{\mathrm{i,max}}$ the maximum interception storage (mm). $S_{\mathrm{i,max}}$ depends on the land cover, and is estimated between $2-8\,\mathrm{mm}$ for a tropical forest (Herwitz, 1985) and between $0-3\,\mathrm{mm}$ for a temperate forest (Gerrits et al., 2010). However, De Boer-Euser et al. (2016) found that the sensitivity of S_{r} to the value of $S_{\mathrm{i,max}}$ is small and, therefore, here a value of $2.5\,\mathrm{mm}$ is used in all catchments for simplicity.

Daily E_{t} ($\mathrm{mm\,day^{-1}}$) in Eq. 2 was calculated by:

$$E_{\mathrm{t}}(t) = c\,E_{\mathrm{p}}(t) \tag{7}$$

where $c\,(-)$ is a coefficient that represents the ratio between transpiration and potential evaporation $c = \overline{E_\mathrm{t}}/\overline{E_\mathrm{p}}$. $\overline{E_\mathrm{t}}\,(\mathrm{mm\,year^{-1}})$ is the long-term mean transpiration derived from the water balance ($\overline{E_\mathrm{t}} = \overline{P_\mathrm{e}} - \overline{Q}$) and $\overline{E_\mathrm{p}}\,(\mathrm{mm\,year^{-1}})$ the long-term mean potential evaporation. E_t considered here includes both transpiration and soil evaporation, but as the latter is much smaller, we use the term transpiration for simplicity. The subtle interactions between atmospheric water demand and vegetation-available water supply can lead to inter-annual variability in c. The above described approach that provided constant estimates of c is therefore extended by an iterative procedure to estimate annually varying values of coefficient c as described in Appendix A.

Catchment $S_\mathrm{r,MM}\,(\mathrm{mm})$ is estimated based on the assumption that a catchment's ecosystem designs its rooting system while keeping memory of water stress events with certain return periods. Previous studies provide evidence that these return periods are likely to be larger for high vegetation (e.g. forest) than for low vegetation (e.g. grass). Based on the results of Gao et al. (2014), De Boer-Euser et al. (2016) and Wang-Erlandsson et al. (2016) drought return periods (RP) for high and low vegetation are set to 40 and 2 years, respectively. The $S_\mathrm{r,MM}$ corresponding to these drought return periods is calculated applying the Gumbel extreme value distribution (Gumbel, 1935) to annual maximum storage deficits. ~~Catchment~~ Theoretically we could treat S_r separately for high and low vegetation in HTESSEL. However, this would require changing the root distributions (see section 2.4), which we decided not to do as we did not want to change multiple parameters at the same time. Therefore, for the implementation of $S_\mathrm{r,MM}$ in HTESSEL, catchment $S_\mathrm{r,MM}$ is estimated as a weighted sum of the high and low vegetation S_r, based on the coverage fraction of high (C_H) and low (C_L) vegetation in the corresponding grid cell of that specific catchment, described by:

$$S_\mathrm{r,MM} = C_\mathrm{L}\,S_\mathrm{r,L,2yr} + C_\mathrm{H}\,S_\mathrm{r,H,40yr} \tag{8}$$

2.4 HTESSEL model description

In this study we use the Hydrology Tiled ECMWF Scheme for Surface Exchanges over Land (HTESSEL) land surface model (Balsamo et al., 2009). This section presents the model parameterization of vegetated areas in the HTESSEL control model version (hereinafter CTR) based on the IFS documentation of cycle CY43R1 and the model codes itself (ECMWF, 2016). The core structure of this model is described by van den Hurk et al. (2000) and major changes in the hydrology parameterization were made by Balsamo et al. (2009) with the implementation of a global soil texture map instead of a single soil type, and a runoff scheme accounting for subgrid variability, which resulted in improvements in global water budget simulations (Balsamo et al., 2011).

Figure 4a represents a simplified 3D view of a single grid cell. The HTESSEL model describes eight different surface fractions within a grid cell (ECMWF, 2016), but we only considered the vegetation covered fractions (high and low vegetation) because of the presence of roots. Considering exclusively vegetated areas, the grid cell surface is subdivided into high and low vegetation covered area (C_H and C_L) with a dominant type of vegetation (T_H and T_L) based on the GLCC1.2 vegetation database. This database distinguishes 18 different vegetation types (e.g. evergreen broadleaf; tall grass; crops), each described with vegetation specific parameters based on experiments and literature (e.g. minimum canopy resistance; root distribution). The subsurface has a single soil texture based on FAO (2003) and is subdivided into four model layers with a total depth z of $2.89\,\mathrm{m}$ that is kept uniformly constant in the global domain.

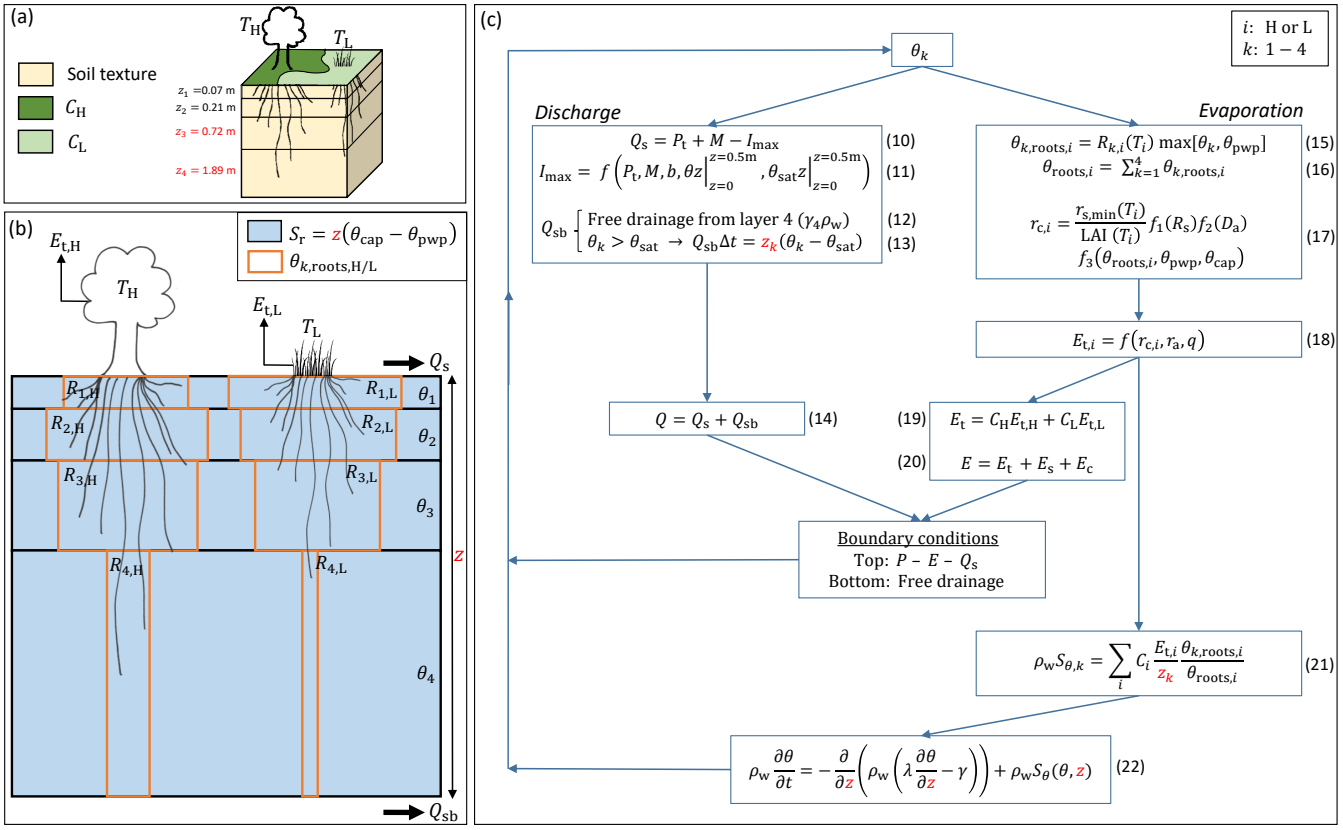

Figure 4. Root zone parameterization in the HTESSEL CTR version with highlighted in red the directly changed parameters in the HTESSEL MD version. (a) 3D overview of a single grid cell. (b) Schematic image of the four layer subsurface. (c) Scheme of equations for the calculation soil moisture, discharge and evaporation. The symbols in this figure are as follows, with i high (H) and low (L) vegetation and k layers 1–4: C $(-)$ vegetation coverage, T dominant vegetation type, z (m) layer depth, P $(\mathrm{m\,s^{-1}})$ precipitation, P_t $(\mathrm{m\,s^{-1}})$ precipitation through-fall, M $(\mathrm{m\,s^{-1}})$ snow-melt, Q $(\mathrm{m\,s^{-1}})$ total discharge, Q_s $(\mathrm{m\,s^{-1}})$ surface runoff, Q_{sb} $(\mathrm{m\,s^{-1}})$ subsurface runoff, I_{max} $(\mathrm{m\,s^{-1}})$ maximum infiltration rate, b $(-)$ variable representing sub-grid orography, E $(\mathrm{m\,s^{-1}})$ total evaporation, E_t $(\mathrm{m\,s^{-1}})$ transpiration, E_s $(\mathrm{m\,s^{-1}})$ soil evaporation, E_c $(\mathrm{m\,s^{-1}})$ canopy evaporation, R (%) root distribution, θ $(\mathrm{m^3 m^{-3}})$ unfrozen soil moisture, θ_{pwp} $(\mathrm{m^3 m^{-3}})$ soil moisture at permanent wilting point, θ_{cap} $(\mathrm{m^3 m^{-3}})$ soil moisture at field capacity, θ_{sat} $(\mathrm{m^3 m^{-3}})$ soil moisture at saturation, S_r (m) the root zone storage capacity, θ_{roots} $(\mathrm{m^3 m^{-3}})$ the root extraction efficiency, r_c $(\mathrm{s\,m^{-1}})$ canopy resistance, r_a $(\mathrm{s\,m^{-1}})$ atmospheric resistance, R_s $(\mathrm{W\,m^{-2}})$ downward shortwave radiation, D_a (hPa) atmospheric water vapour deficit, q specific humidity $(\mathrm{kg\,kg^{-1}})$, $r_{s,min}$ $(\mathrm{s\,m^{-1}})$ minimum canopy resistance, LAI $(-)$ Leaf Area Index, S_θ $(\mathrm{m^3 m^{-3} s^{-1}})$ root extraction rate, γ $(\mathrm{m\,s^{-1}})$ hydraulic conductivity, λ $(\mathrm{m^2 s^{-1}})$ hydraulic diffusivity and ρ_w $(\mathrm{kg\,m^{-3}})$ density of water.

Figure 4b presents the connection of the subsurface with the surface, through roots and transpiration fluxes (E_t) in more detail. S_r is not explicitly described in the model parameterization and, therefore, it is formulated based on our own under-

standing of its relation to the HTESSEL vegetation and root zone parameterizations (Eq. 9). Vegetation has roots in all four model soil layers (except for vegetation types desert and tundra that can only access the upper layer and the upper three layers, respectively (ECMWF, 2016)). There is a variable root distribution across the layers that is different for each vegetation type. The vegetation specific root distribution (R_k) describes the root fraction with respect to the total amount of roots in each model soil layer. At a single time step, the capability of roots to extract soil moisture ($\theta_{k,\mathrm{roots}}$, represented by the brown boxes in 4b) is a function of R_k and the layer unfrozen soil moisture content (θ_k). Thus, the more roots we have in a soil layer, the more moisture can be extracted at each time step. In the long term, however, the vegetation is able to extract all the plant available soil moisture in the layers where roots are present. Therefore, $S_{\mathrm{r,CTR}}$, represented in blue in Fig. 4b, is described by:

$$S_{\mathrm{r,CTR}} = z(\theta_{\mathrm{cap}} - \theta_{\mathrm{pwp}}) \tag{9}$$

with z ~~the~~ representing the hydrologically active depth which corresponds to the combined depth of all soil layers with roots ($z = 2.89$ m is a default value in HTESSEL for all vegetation types except for desert and tundra), and $\theta_{\mathrm{cap}} - \theta_{\mathrm{pwp}}$ the plant available moisture which is constant over the four soil layers. The plant available moisture is bounded by the soil texture specific moisture contents at field capacity (θ_{cap}), above which soil moisture drains by gravity, and at wilting point (θ_{pwp}), below which soil moisture is not accessible to roots. ~~Runoff from the system occurs as surface runoff (Q_{s}) and subsurface runoff (Q_{sb})~~It should be noted that we aimed for a physical definition of $S_{\mathrm{r,CTR}}$, but that the effective water used by vegetation may be different. We come back to this point more elaborately in the discussion (Sect. 4.3).

Figure 4c presents the equation scheme of HTESSEL for calculating soil moisture and discharge and evaporation fluxes, with i high (H) or low vegetation cover (L) and k the four soil layers. The relative soil moisture content θ controls the calculations of discharge and evaporation fluxes. The surface runoff (Q_{s}) is defined by the precipitation through-fall (P_{t}), snow-melt (M) and the maximum infiltration rate (I_{max}) (Eq. ~~9~~10). I_{max} is a function of P_{t}, M, a spatially variable parameter (b), that is defined by the standard deviation in sub-grid orography, and the vertically integrated (top 0.5 m) soil moisture (θ) and saturation soil moisture (θ_{sat}) (Eq. ~~10~~11) (Dümenil and Todini, 1992; van den Hurk and Viterbo, 2003). The subsurface runoff (Q_{sb}) consists of two components: free drainage from layer 4, that is a function of hydraulic conductivity in this layer (γ_4) and water density (ρ_{w}) (Eq. ~~11~~12) and the excess absolute soil moisture when $\theta_k > \theta_{\mathrm{sat}}$ (Eq. ~~12~~13). Total discharge (Q) is the sum of Q_{s} and Q_{sb} (Eq. ~~13)~~14), and as typical in-stream travel times through the catchments are about 1 day at most, we did not consider routing to be important at the monthly time scale for which we analyze the results. The average root extraction efficiency in all layers (θ_{roots}) is described by Eq. ~~14~~ 15 and Eq. ~~15~~ 16 as the weighted sum of the vegetation specific R_k and θ_k. The canopy resistance (r_{c}) (Eq. ~~16~~17) describes the resistance of vegetation to transpiration and is a function of vegetation specific values for minimum canopy resistance ($r_{\mathrm{s,min}}$) and LAI, a function of shortwave radiation ($f_1(R_{\mathrm{s}})$), a function of atmospheric water vapour deficit ($f_2(D_{\mathrm{a}})$) and a function of the root extraction efficiency ($f_3(\theta_{\mathrm{roots},i}, \theta_{\mathrm{pwp}}, \theta_{\mathrm{cap}})$. The canopy resistance defines $E_{\mathrm{t,i}}$ together with specific humidity (q) and an atmospheric resistance term (r_{a}) (Eq. ~~17~~18). Total E_{t} is a weighted sum of the separate transpiration products based on the sub-grid coverage C_{L} and C_{H} (Eq. ~~18~~19) and total evaporation (E) is a sum of transpiration (E_{t}), soil evaporation (E_{s}) and canopy evaporation (E_{c}) fluxes (Eq. ~~19~~20). The detailed formulations of the latter two fluxes are not relevant in this study and, therefore, not included in this model description. $E_{\mathrm{t,i}}$ is attributed to the different

soil layers in the calculation of the root extraction (S_θ) based on the layer depth (z_k) and $\theta_{k,\text{roots}}$ (Eq. ~~20~~21). The change in soil moisture over time ($\partial\theta/\partial t$) is calculated applying the Darcy-Richards equation with γ and λ hydraulic conductivity and diffusivity (Eq. ~~21~~22). This equation is solved with top soil boundary condition of $P - E - Q_s$, and a bottom soil boundary condition of free drainage.

2.5 Implementation of memory method root zone storage capacity estimates in HTESSEL

Here we develop an approach to implement the climate controlled $S_{r,MM}$ (results in Sect. 3.1) in HTESSEL, while maintaining the modeling framework of the CTR model described in Sect. 2.4. We found that $S_{r,CTR}$ is exclusively defined by the soil type and the hydrologically active model soil depth (z) (Eq. 9). In our modified version of HTESSEL, hereafter referred to as the Moisture Depth (MD) model, the soil depth for moisture calculations is changed to satisfy the following equation:

$$S_{r,MD} = S_{r,MM} = z_{MD}(\theta_{cap} - \theta_{pwp}) \tag{23}$$

with z_{MD} the total soil depth in the MD model modified to satisfy $S_{r,MD} = S_{r,MM}$. This depth change is achieved by changing model layer 4, except in the case this would ~~lead~~ cause the model depth of layer 4 to approach zero ($z_4 \approx 0$). In this case a minimum threshold (0.2 m) is set for z_4 and the depth of layer 3 is further changed to obtain $S_{r,MD}$ = $S_{r,MM}$ as required in Eq. 23. This is necessary because $z_4 \approx 0$ in the moisture calculation would cause inconsistencies in the thermal diffusion calculations as the layer soil temperature is a function of the layer soil moisture. ~~It should be noted that the~~ The layer depths for thermal diffusion calculations are not modified in the MD model and we found that the soil layer temperatures are insensitive to depth changes in MD. The directly changed parameters in MD are highlighted in red in Fig. 4. Also, the root distribution is not modified in MD, because we aimed for a physical representation of S_r (Eq. 23) and we did not want to change multiple model parameters at the same time. Furthermore, we would like to re-iterate that the soil depth in the model should neither be interpreted as actual soil depth nor rooting depth, but merely as a way to represent the plant accessible water volume.

2.6 Model simulations

Simulations are performed in a standalone version of HTESSEL (Balsamo et al., 2009) as it was implemented in the frame of version 3 of the EC-EARTH Earth system model (http://www.ec-earth.org) for both the CTR (Sect. 2.4) and MD (Sect. 2.5) model versions. The model is forced with 3-hourly GSWP-3 atmospheric boundary conditions (Kim, 2017) for the historical time series 1970–2010, with the first five years used for spin-up. The spatial resolution of the HTESSEL model is a reduced gaussian grid (N128), with the grid cells over Australia being approximately 5500 km^2.

2.7 Model evaluation

Most study catchments are smaller than single HTESSEL grid cells (Table S1). For catchments completely falling within a single HTESSEL grid cell, this cell is selected for analysis. In the case a catchment falls within more than one grid cell, the average of the model output in the separate grid cells is used for analysis. The model performances of CTR and MD are compared based on modeled monthly discharge and evaporation fluxes for 1975–2010: long-term annual means, monthly

seasonal climatology and inter-annual anomalies of monthly fluxes (monthly fluxes minus monthly climatology) are evaluated. Modeled Q is compared to station observations and modeled E to the FLUXCOM-WB evaporation (Sect. 2.2 and Eq. 1). For long-term annual means, the percent-bias between the reference and modeled fluxes is calculated (evaporation p-bias $= (\overline{E}_{\text{mod}} - \overline{E}_{\text{ref}})/\overline{E}_{\text{ref}}$). For the monthly seasonal climatology and inter-annual anomalies, the model performance is quantified by using the Pearson correlation coefficient (r) and a variability performance metric ($v = (1-\alpha)^2$) that depends on the ratio of modeled and reference standard deviation ($\alpha = \sigma_{\text{mod}}/\sigma_{\text{ref}}$). These performance metrics are calculated for the individual catchments, and then averaged to evaluate model performance over tropical, temperate and Mediterranean climate regions.

To test significance of the improvement in model performance of MD compared to CTR, a Monte Carlo bootstrap method (1000 repetitions) is employed. The 1000 samples are taken by resampling randomly with replacement among CTR and MD values at each time-step. The null hypothesis of getting as high or higher performance parameters simply by chance is tested at the 5% and 10% significance levels, for the individual catchments as well as for the performance averages over the tropical, temperate and Mediterranean climate regions. P-values of the model improvements are provided in the Supplementary Material (Tables S5 and S6).

3 Results

3.1 Root zone storage capacity estimates

Figure 5 shows that there is no relation between $S_{\text{r,MM}}$ and $S_{\text{r,CTR}}$. The range of $S_{\text{r,MM}}$ (125–722 mm) in the study catchments is much larger than the range of $S_{\text{r,CTR}}$ (491–725 mm), indicating that HTESSEL may not adequately represent the spatial heterogeneity of S_{r} (Table S2). The range of $S_{\text{r,MM}}$ in the catchments is consistent with Wang-Erlandsson et al. (2016), who found similar ranges of S_{r} (approximately 100–600 mm) over Australia by using gridded products of S_{r} based on rooting depths from observations and optimised inverse modelling, and global $S_{\text{r,MM}}$ estimated based on satellite evaporation products. $S_{\text{r,MM}}$ estimates are on average smaller in the five temperate (194 mm) catchments than in the three Mediterranean (321 mm) and the seven tropical (437 mm) catchments. In the tropical and Mediterranean regions vegetation needs to bridge extensive dry seasons as rainfall seasonality is high (Fig. 2, Table 1), resulting in larger $S_{\text{r,MM}}$ than in temperate regions with year-round precipitation. In the Mediterranean, the average time-lag between P and E_{p} of 5.7 months results in large root zone storage deficits in the hot and dry summers, and therefore, larger $S_{\text{r,MM}}$ than in the temperate catchments.

3.2 Long-term mean annual climatology

The HTESSEL CTR version overestimates observed $\overline{Q}$ in 9 out of 15 catchments with on average 40 mm year^{-1} (tropical), 3 mm year^{-1} (temperate) and 122 mm year^{-1} (Mediterranean) (Table 2; Table S3; Table S4). This overestimation of observed Q goes together with an average underestimation of $\overline{E}_{\text{WB}}$ by CTR. As $S_{\text{r,MM}}$ is generally smaller than $S_{\text{r,CTR}}$ (Fig. 5), the MD version results in reduced $\overline{E}$ and increased $\overline{Q}$ compared to CTR, but the changes are quite small (Table 2). The MD increase in modeled $\overline{Q}$ compared to CTR results on average in larger p-biases in tropical (+16.9 % vs. +13.7 %), temperate (+24.4 %

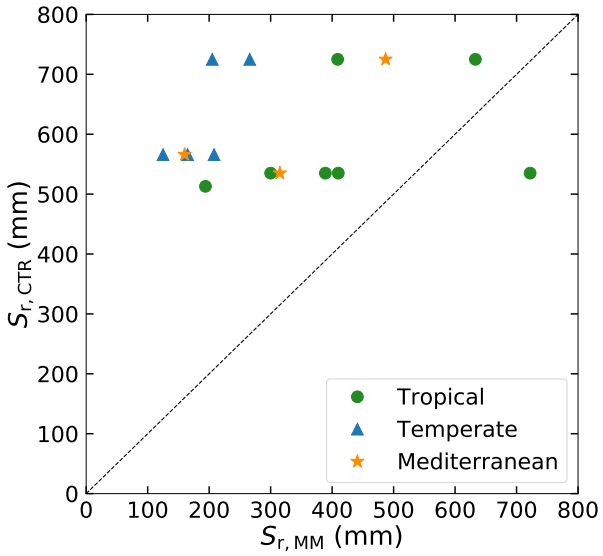

Figure 5. Catchment S_r as estimated from the memory method ($S_{r,MM}$) compared to the HTESSEL CTR parameterization ($S_{r,CTR}$) in the catchment corresponding grid-cells.

285 vs. +4.9 %) and Mediterranean (+263.8 % vs. +249.9 %) catchments, but the results are largely variable among the individual catchments (Table S4).

Table 2. Long-term annual mean modeled discharge ($\overline{Q}$) and evaporation ($\overline{E}$) in the HTESSEL CTR and MD versions for the tropical, temperate and Mediterranean climate regions (catchment averages) and reference $\overline{Q}$ (station observations) and $\overline{E}$ ($\overline{E}_{WB}$ (Sect. 2.2)). The p-biases of the modeled climate region average $\overline{Q}$ and $\overline{E}$ are presented between brackets. Similar values for the individual catchments are shown in Tables S3 and S4.

	$\overline{Q}$ (mm year^{-1})			$\overline{E}$ (mm year^{-1})		
Climate region	Observations	HTESSEL CTR	HTESSEL MD	WB	HTESSEL CTR	HTESSEL MD
Tropical	291	331 (+13.7%)	~~340~~ 345 (+~~16.9~~18.6%)	834	790 (-5.3%)	~~781~~ (-6.5~~776~~ (-7.1%)
Temperate	56	59 (+4.9%)	70 (+24.4%)	626	624 (-0.4%)	611 (-2.4%)
Mediterranean	49	171 (+249.9%)	177 (+263.8%)	836	717 (-14.2%)	709 (-15.2%)

3.3 Monthly seasonal climatology

Although $\overline{Q}$ does not considerably change in MD compared to CTR (Sect. 3.2), MD reproduces the seasonal variations in Q considerably better than CTR (Fig. 6a–c and Table 3). In the tropical and Mediterranean catchments, MD increases Q in the

wet months while it decreases Q in the dry months compared to CTR, and hence improves the seasonal timing of observed Q (Fig. 6a,c and Table 3). In the temperate catchments, MD increases Q in the wet months (Jul–Sep) compared to CTR in accordance with observations, although in the other months the changes of MD compared to CTR are mixed (Fig. 6b). In terms of the correlation between modeled and observed monthly seasonal climatology, Q improved in MD compared to CTR in 12 out of 15 catchments, with 7 catchments passing the 5% significance level for improvement (Table S5). For the climate region averages, the correlation significantly improved in MD from 0.84 to 0.90 (tropical), from 0.74 to 0.86 (temperate) and from 0.86 to 0.96 (Mediterranean) compared to CTR (Table 3). On average, MD resulted in larger variations in monthly Q than CTR (Fig. 6a–c). The variability term $v = (1 - \sigma_{\text{mod}}/\sigma_{\text{obs}})^2$ improved from 0.17 to 0.06 (tropical) and from 0.17 to 0.10 (temperate) in MD compared to CTR, but in the Mediterranean catchments the models strongly overestimate the observed variations in Q (Fig. 6c) with the variability term increasing from 2.80 in CTR to 8.73 in MD (Table 3; Table S5).

In contrast to the improvement in monthly seasonal climatology of Q in MD, the monthly seasonal cycle of E appears to be not much affected as ~~reported~~ shown in Fig. 6d–f and Table 3.

Table 3. Model performance parameters of monthly seasonal discharge (Q) and evaporation (E) climatologies (1975–2010), with r representing pearson correlation and $v = (1 - \alpha)^2$ variability, with $\alpha = \sigma_{\text{mod}}/\sigma_{\text{obs}}$, in tropical, temperate and Mediterranean climate regions for the HTESSEL CTR and MD versions (catchment averages). Modeled Q is compared to station observations and modeled E to FLUXCOM-WB (Eq. 1). For r, a value of 1 represents a perfect model, for v a value of 0 represents a perfect model. The significance test of the MD improvements compared to CTR is represented by ** (passing 5% level) and * (passing 10% level). Values of r and α for the individual catchments and p-values of improvement are shown in Tables S5 (Q) and S6 (E).

		Discharge		Evaporation	
Climate region	HTESSEL version	r (-)	v (-)	r (-)	v (-)
Tropical	CTR	0.84	0.17	0.98	0.07
	MD	0.90**	0.05**	0.98	0.07
Temperate	CTR	0.74	0.17	0.99	0.04
	MD	0.86**	0.10**	0.98	0.05
Mediterranean	CTR	0.86	2.80	0.81	0.08
	MD	0.96*	8.73	0.80	0.07

3.4 Inter-annual monthly anomalies

Figure 7a and 7c show that MD is better in capturing the variations in inter-annual Q anomalies than CTR in the presented tropical and temperate catchments, while in the Mediterranean catchment both models strongly overestimate the inter-annual Q anomalies compared to observations (Fig. 7e). In 14 out of 15 catchments, the variability in the inter-annual Q anomalies

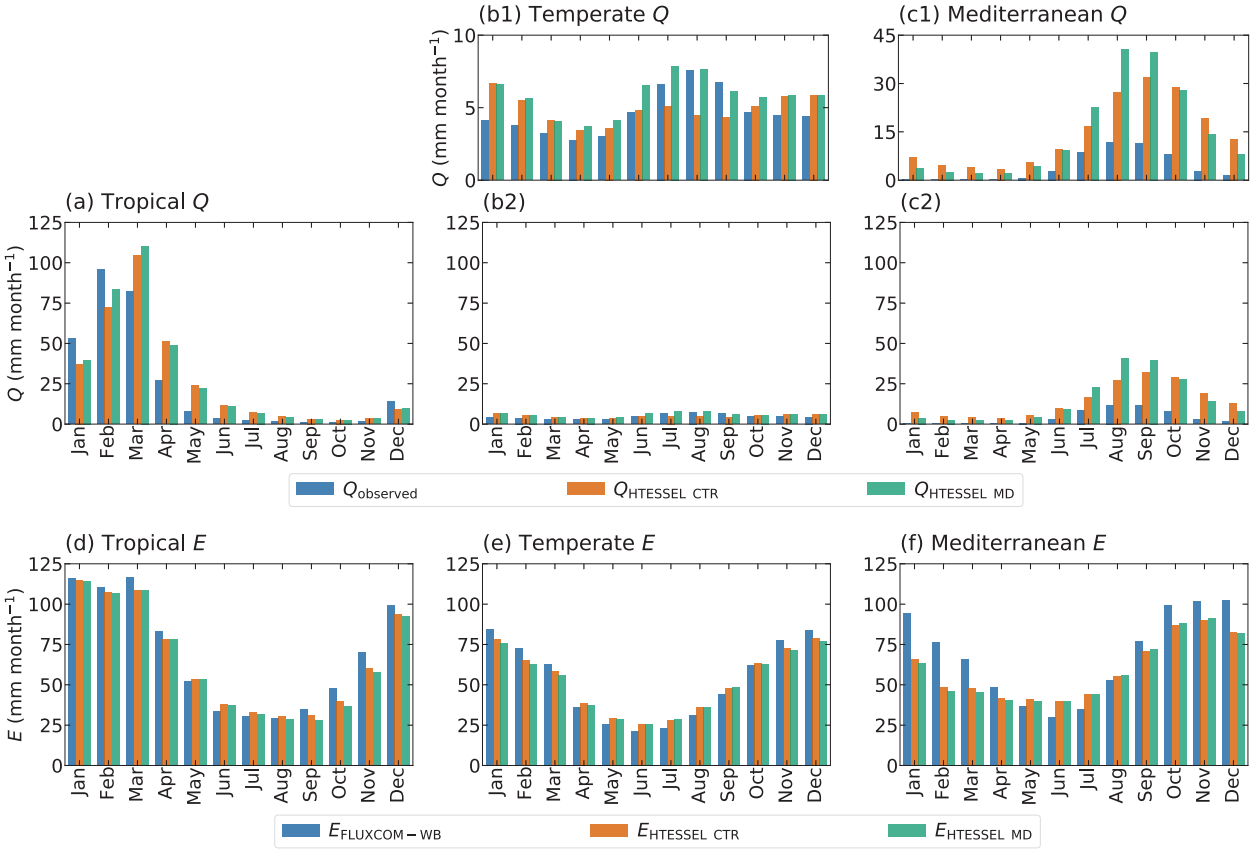

Figure 6. Monthly seasonal climatology of observed discharge (Q) (top) and FLUXCOM-WB evaporation ($E_{\text{FLUXCOM-WB}}$) (bottom) and modeled values in the HTESSEL CTR and MD versions, averaged for the tropical (a, d), temperate (b, e) and Mediterranean (c, f) catchments for the time series 1975–2010. b1 and c1 represent the same data as b2 and c2, but with a different y-axis. Similar figures for the individual catchments are shown in Fig. S1 (Q) and Fig. S2 (E).

increases in MD compared to CTR (Fig. S1; Table S5). This results in an average improvement in the inter-annual anomaly variability (v) from 0.12 to 0.11 (tropical) and from 0.09 to 0.06 (temperate) in MD compared to CTR (Table 4). However, in the Mediterranean catchments, the increased variability in the Q anomalies leads to a strong overestimation of Q anomalies with respect to observations (Fig. 7e; Fig. S1m–o), with v increasing from 0.99 in CTR to 4.26 in MD. Figures 7a, 7c and 7e also show that the timing of the Q anomalies improves in MD compared to CTR, with in particular the improved timing of the falling limbs clearly visible in Fig. 7a and 7e. The inter-annual Q anomaly correlation (corresponding to the timing) improves in 14 out of 15 catchments, with 9 catchments passing the 5% significance level for improvement (Table S5). On average, the correlation (r) increases from 0.74 to 0.78 (tropical), from 0.80 to 0.85 (temperate) and from 0.71 to 0.79 (Mediterranean) in

Table 4. Model performance parameters of inter-annual monthly discharge (Q) and evaporation (E) anomalies (1975–2010), with r representing pearson correlation and $v = (1-\alpha)^2$ variability, with $\alpha = \sigma_{\text{mod}}/\sigma_{\text{obs}}$, in tropical, temperate and Mediterranean climate regions for the HTESSEL CTR and MD versions (catchment averages). Modeled Q is compared to station observations and modeled E to FLUXCOM-WB (Eq. 1). For r, a value of 1 represents a perfect model, for v a value of 0 represents a perfect model. The significance test of the MD improvements compared to CTR is represented by ** (passing 5% level) and * (passing 10% level). Values of r and α for the individual catchments and p-values of improvement are shown in Tables S5 (Q) and S6 (E).

		Discharge		Evaporation	
Climate region	HTESSEL version	r (-)	v (-)	r (-)	v (-)
Tropical	CTR	0.74	0.12	0.79	1.39
	MD	0.78**	0.11	0.80**	1.52
Temperate	CTR	0.80	0.09	0.81	1.12
	MD	0.85**	0.06*	0.82**	1.46
Mediterranean	CTR	0.71	0.99	0.78	1.17
	MD	0.79**	4.26	0.78	1.31

MD compared to CTR. In contrast to the improvement in the inter-annual Q anomalies in MD, the inter-annual E anomalies do not considerably change compared to CTR (Fig. 7b,d,f; Table 4, Table S6).

4 Discussion

4.1 Synthesis of results

$S_{\text{r,MM}}$ is lower than $S_{\text{r,CTR}}$ in 14 out of 15 catchments (Fig. 5). This is seemingly in contrast with literature suggesting that the root depth in land surface models is too low and that the absence of deep roots is a cause for uncertainties in simulated evaporation (Kleidon and Heimann, 1998; Pan et al., 2020; Sakschewski et al., 2020). However, S_{r} represents ~~the water volume~~ a conceptual water volume that is accessible to roots ~~and is therefore~~ without defining where this volume is in reality. Therefore, it is not necessarily proportional to root depth as a small S_{r} does not preclude the presence of deep roots, as illustrated in Fig. 4 in Singh et al. (2020).

The modeling results show that the difference in long-term mean $\overline{Q}$ and $\overline{E}$ fluxes between CTR and MD are small (Table 2), whereas the differences between monthly (climatological and inter-annual) variations are clearly visible (Fig. 6 and Fig. 7). This corresponds to other studies on catchment hydrology that suggest that the root zone storage mainly affects the fast hydrological response of a catchment (Oudin et al., 2004; Euser et al., 2015; Nijzink et al., 2016; De Boer-Euser et al., 2016). Furthermore, previous studies found larger improvements of modeled discharge using $S_{\text{r,MM}}$ in humid regions with large rainfall

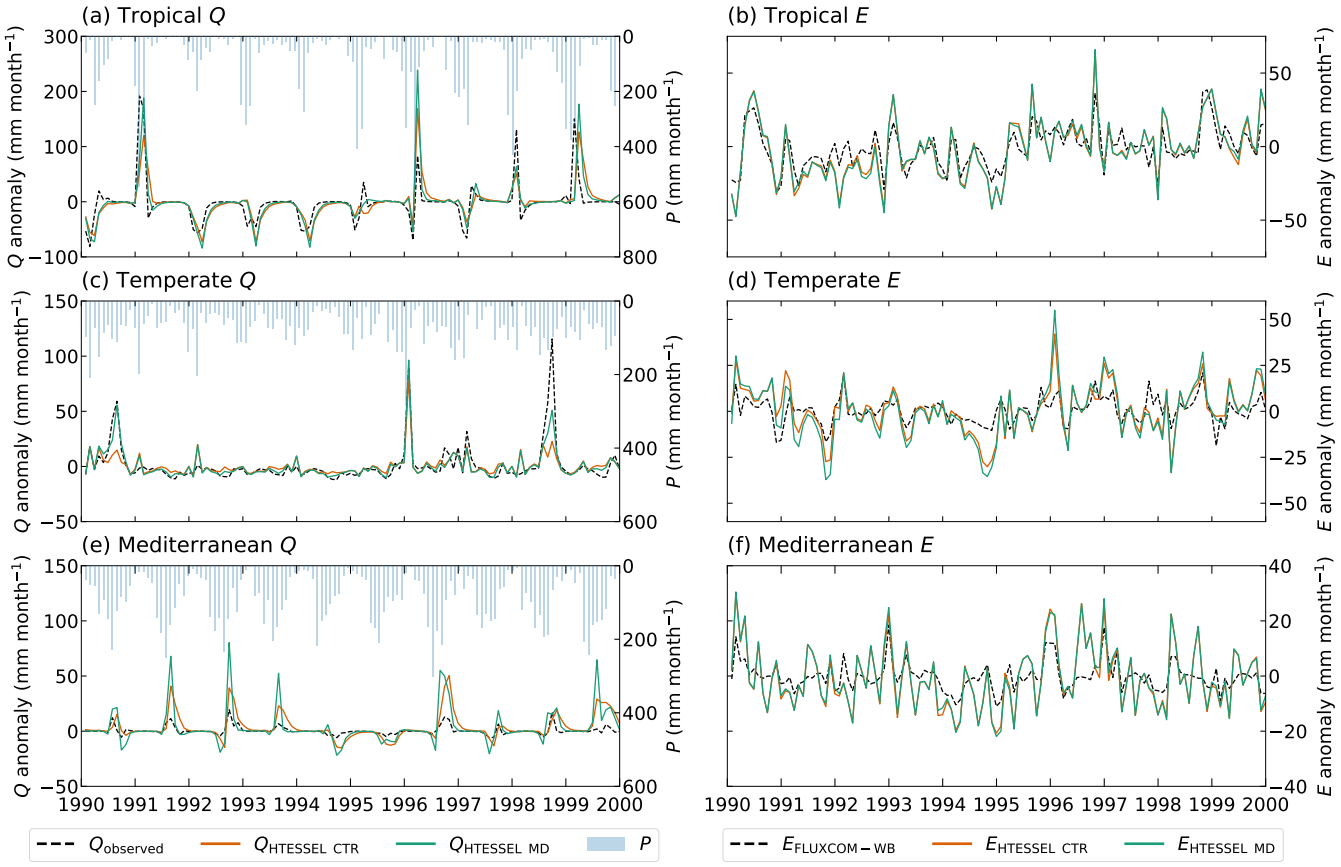

Figure 7. Inter-annual monthly anomalies of observed discharge (Q) (left) and FLUXCOM-WB evaporation (E) (right) fluxes and modeled values in the HTESSEL CTR and MD versions, in an individual representative tropical (catchment Mi) (a, b), temperate (catchment Na) (c, d) and Mediterranean (catchment K) (e, f) catchment based on the time series 1975–2010. Similar figures for the individual catchments are shown in Fig. S1 (Q) and Fig. S2 (E).

seasonality (De Boer-Euser et al., 2016; Wang-Erlandsson et al., 2016). This is not found in our study, as we obtain slightly smaller improvements in the discharge correlation for the tropical catchments than for the temperate and Mediterranean ones. This is at least partly related to the smaller difference between $S_{r,MM}$ and $S_{r,CTR}$ in the tropical catchments than in temperate and Mediterranean ones (Fig. 5). The Mediterranean catchments have large climatological biases and too large discharge variability in the seasonal cycle and inter-annual anomalies in CTR, and MD further degrades the performance with respect to bias and variability (Tables 2, 3 and 4). On the other hand, the correlation of seasonal climatology and inter-annual anomalies consistently improves in all climate regions with the implementation of $S_{r,MM}$. Therefore, it is suggested that other aspects of the hydrology parameterization than S_r (e.g. the lack of a groundwater layer) could be primarily leading to the large climatological biases and too large discharge variability in the seasonal cycle and inter-annual anomalies in the Mediterranean. On the other hand, uncertainties in the GSWP-3 forcing could also in part cause the large biases in the Mediterranean. In this climate region,

it is found that GSWP-3 $\overline{P}$ (0.5°grid) is considerably larger than $\overline{P}$ from the SILO dataset, that provides P on a 0.05°grid directly derived from ground-based observational data (Jeffrey et al., 2001).

Although we found significant differences in modeled Q between CTR and MD, the discrepancy in E was very limited in all climate regions (Table 3; Table 4; Table S6; Fig. S2). ~~This~~ As stated before, the reliability of the FLUXCOM E is questionable in our study catchments (Fig. 3). Although the model performance with respect to E fluxes is uncertain, the lack of evaporation sensitivity to S_r ~~is~~ was unexpected and requires more in depth evaluation of ~~HTESSEL. In this respect, it would be useful to check how this insensitivity of evaporation to~~ the results in view of the HTESSEL model parameterization.

In order to further explain the evaporation (in)sensitivity we analyzed the modelled soil moisture, and specifically looked at a wet period (mid 1990) and a dry period (start 1991) in a temperate catchment, as shown in Fig. 8b. During the wet period, soil moisture in the upper three layers is above or close to θ_{cap} for both MD and CTR, while in the fourth layer MD has larger soil moisture than CTR. In this case evaporation is not moisture limited and controlled by the top three layers because of the larger root distribution in these layers (Eq. 14 and Eq. 15). Therefore, the modelled transpiration is not sensitive to the increase in layer 4 soil moisture in MD compared to CTR. During the transition from wet to dry periods, the upper three layers dry out first as there is a reduction in precipitation input. As these layers are relatively dry, evaporation is controlled by the fourth layer in which θ reduces to values close to θ_{pwp} in MD, while it remains relatively wet in CTR. It is this difference in θ_4 that causes the sensitivity of transpiration in MD during the wet to dry transition. However, most of the time the modelled soil moisture is in the wet and insensitive regime, and, therefore, the overall effect of MD on modelled evaporation tend to be small in the catchments considered in this study. To further analyse the evaporation sensitivity to S_r changes, it would be useful to evaluate to what extent it is model dependent and compare HTESSEL behavior with other LSMs in a multi-model context ~~, comparable to for example~~ (e.g. van den Hurk et al. (2016) and Ardilouze et al. (2017)). On the other hand, we also expect ~~this to~~ the evaporation sensitivity to S_r to be related to methodology applied which will be further discussed in Section 4.3.

4.2 Methodological uncertainty

Although the catchments were selected carefully, their location and sizes do not completely match with the HTESSEL grid cells. Thus, assuming a one to one relation between precipitation, evaporation, river discharge and root zone storage capacities at the catchment and the grid cell is a potential source of error. However, this configures as random error and is therefore likely to cancel out in multiple catchment settings as is done in this study. Another source of uncertainty is the parameterization of the memory method for estimating catchment S_r. This method requires estimations of maximum interception storage, seasonal and inter-annual transpiration signals and return periods, which lead to differences in $S_{r,MM}$ when other values are chosen. A sensitivity analysis of $S_{r,MM}$ with a high $S_{r,MM}$ ($S_{i,max} = 1.5\,mm$, $RP_{low} = 3\,years$, $RP_{high} = 60\,years$, $f = 0.15$ (see Appendix A)) and a low $S_{r,MM}$ ($S_{i,max} = 3.5\,mm$, $RP_{low} = 1.5\,years$, $RP_{high} = 20\,years$, $f = 0.35$) on average deviated $45\,mm$ from the average $S_{r,MM}$ estimates used in this study ($S_{i,max} = 2.5\,mm$, $RP_{low} = 2\,years$, $RP_{high} = 40\,years$, $f = 0.25$). This deviation is small considering the average $S_{r,MM}$ being $319\,mm$. Besides, irrigation, as a possible external water source in catchments with crops (Table S1), and deep groundwater, as a water source for deep-rooting vegetation, are not accounted for in the approach. However, we think that the estimation of transpiration is the main uncertainty in the approach. The assumption that the seasonal

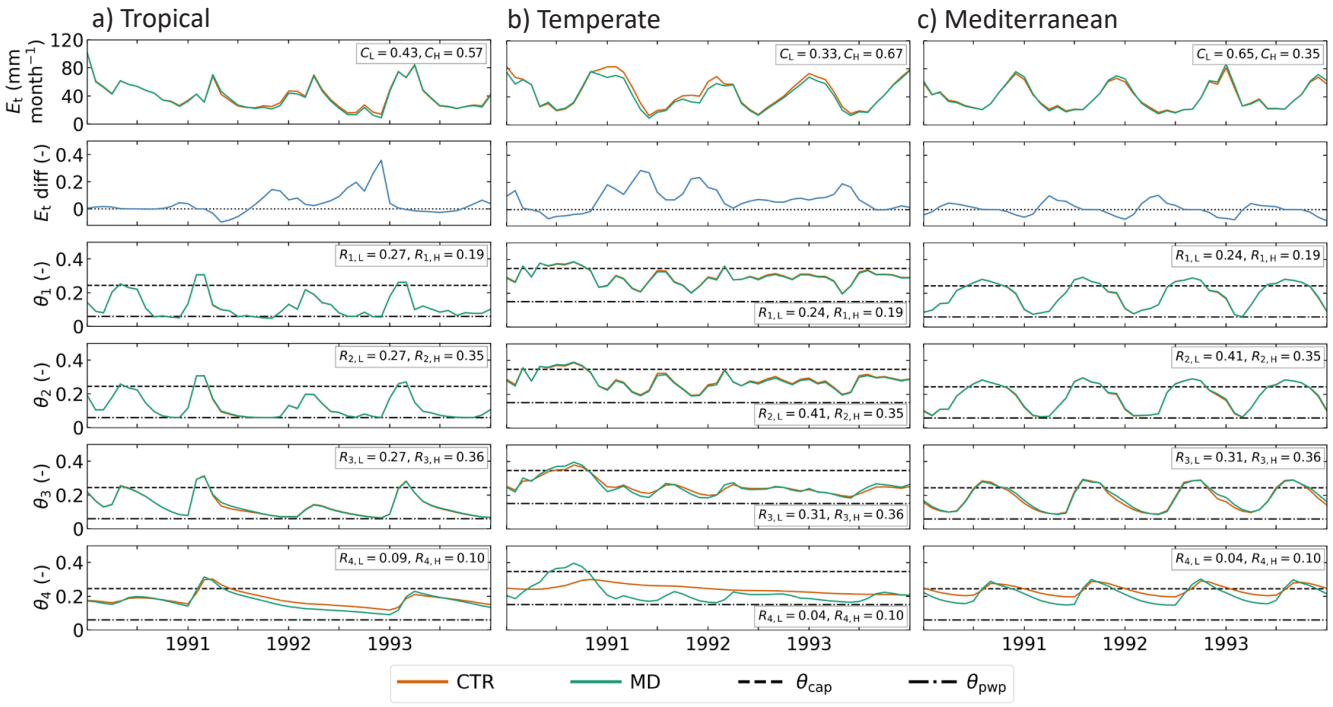

Figure 8. Modelled transpiration and soil moisture content in the HTESSEL CTR and MD versions in an individual representative tropical (catchment Mi) (a), temperate (catchment Na) (b) and Mediterranean (catchment K) (c) catchment. From top to bottom: transpiration, relative difference between CTR and MD transpiration ($\frac{E_{t,CTR} - E_{t,MD}}{E_{t,CTR}}$), soil moisture layer 1, soil moisture layer 2, soil moisture layer 3, soil moisture layer 4. Additionally, the vegetation coverage (C_L and C_H) and the relative rooting distribution (R_k) for the dominant high and low vegetation types are presented.

variations in E_t and E_p are in phase may not hold in Mediterranean regions where E_p and P, and thereby the water available for transpiration, tend to be out of phase. Applying the seasonal pattern of transpiration modeled by CTR to the memory method in Mediterranean catchments results in smaller $S_{r,MM}$ estimates in these catchments (average: 292 mm) than with the initial approach where the seasonality of E_t was based on E_p (average: 321 mm). The relatively low deviation for both the parameter uncertainty and the uncertainty in the timing of E_t leads us to conclude that these assumptions have a small impact on the general finding that $S_{r,MM}$ is lower than $S_{r,CTR}$ and that HTESSEL does not represent the spatial heterogeneity of S_r.

Station observations of river discharge are used in both the $S_{r,MM}$ estimation and the model evaluation. However, because the memory method is only based on observations of long term annual mean discharge ($\overline{Q}$) and the model evaluation is mainly based on the monthly seasonal and inter-annual variations in Q, we consider model evaluation based on these data appropriate.

4.3 Root zone storage capacity implementation

The HTESSEL CTR version does not explicitly formulate S_r and, therefore, we formulate $S_{r,CTR}$ based on the root zone parameterization as presented in Sect. 2.4 in order to modify the model parameters in a way to make the model consistent with the $S_{r,MM}$ estimates. This formulation represents the theoretical $S_{r,CTR}$, but it ~~remains uncertain to what extent~~ may not fully correspond to the soil moisture in the four layers that is actually used by the modeled vegetation~~, in particular in layer 4 because of the~~. The effective S_r ($S_{r,CTR,eff}$) can be derived a posteriori from the modelled soil moisture storage deficits and an extreme value analyses as done in the memory method (Sect. 2.3). $S_{r,CTR,eff}$ is smaller than $S_{r,CTR}$ based on depths (Fig. S3c), which is likely related to the relatively small root percentage ~~prescribed from look-up tables in this layer~~ in layer 4 compared to the other layers for most vegetation types ~~compared to the other layers.~~ (ECMWF, 2016). On the other hand, the $S_{r,MM}$ we implemented in MD by changing soil depths is close the $S_{r,MD,eff}$ based on modelled soil moisture deficits in MD (Fig. S3d).

In MD the depths for soil moisture calculations are changed, directly resulting in changes in absolute soil moisture and, thereby in indirect changes in discharge and transpiration. This modification is relatively simple, flexible and there is no limitation in the possible range of soil depths for moisture calculations and, therefore, could similarly be implemented in other land surface models. However, it should be noted that this strategy chosen for changing the HTESSEL S_r is not the only possible. As follows from Eq. 9, also the plant available soil moisture ($\theta_{cap} - \theta_{pwp}$) defines the S_r. However, modifications in the model's θ_{cap} or θ_{pwp} are not desired as these parameters are soil texture specific properties. Moreover, modifications in the formulations of the root available moisture for each time-step (θ_{roots}) appears conceptually not meaningful.

There are several alternative hypotheses that may potentially explain the limited sensitivity of modeled E to the modified S_r. First, the resistance of vegetation to transpiration is a function of the moisture supply (soil moisture) and the moisture demand (atmospheric condition) (Eq. 14–16). The atmospheric conditions, that define moisture demand and thereby constrain transpiration, are similar in both CTR and MD because the models are run in an offline version. Therefore, the soil moisture-atmosphere feedback is not represented and the moisture demand side dominates the moisture supply side in the evaporation calculations. This issue could be overcome by using coupled climate simulations. Second, although S_r is changed in MD compared to CTR, the parameterization of the vegetation water stress is kept constant. Ferguson et al. (2016) found that different formulations of root water uptake considerably influence modeled water budgets and, therefore, it is likely that changes in evaporation in MD compared to CTR are constrained by the vegetation water stress formulations (Eq. 14–16). Third, the insensitivity of evaporation to the changes in model soil depth is probably also related to the fact that the resistance of vegetation to transpiration is a function of the relative soil moisture (θ), which is not directly affected by changing the soil depth. On the other hand, soil depth changes directly affect the modeled Q, as modeled surface (Q_s) and subsurface runoff (Q_{sb}) directly depend on the absolute moisture storage capacity of the soil (see Eq. 10 and Eq. 12), with Q_s a function of the absolute moisture in the top 50 cm of soil and Q_{sb} a function of the the ~~absolute~~ total excess soil moisture when the layer's moisture content exceeds saturation moisture content. Fourth, monthly fluxes of Q are often a full order of magnitude smaller than E. Hence small changes in the partitioning simply add up to larger relative changes for Q.

5 Conclusions

This study is an attempt to overcome major limitations in the representation of the vegetation's root zone in land surface models. Specifically, we looked at the HTESSEL land surface model and found that the root zone storage capacity S_r is only ~~as~~ a function of soil texture and soil depth, the latter being kept constant over the modeled global domain (in HTESSEL $z = 2.89\,\mathrm{m}$), while from the state-of-the-art literature (e.g. Collins and Bras, 2007; Guswa, 2008; Gentine et al., 2012; Gao et al., 2014) it is indicated that S_r is, to a large extent, climate controlled. We found that indeed the HTESSEL control version (CTR) does not adequately represent the spatial heterogeneity of S_r, with the range of $S_{r,CTR}$ (491–725 mm) much narrower than the range obtained for the climate controlled estimate $S_{r,MM}$ (125–722 mm) in 15 Australian catchments with contrasting climate characteristics considered in this study. Furthermore, $S_{r,CTR}$ was found to be considerably larger than the climate controlled estimate $S_{r,MM}$ in 14 out of 15 catchments. It is noted that these findings could be different for other LSMs when they have shallower soil depths.

We developed a new version of HTESSEL by suitably modifying the soil depths (MD) to obtain modeled $S_{r,MD}$ that matches $S_{r,MM}$ over the 15 catchments considered over Australia, while maintaining the overall HTESSEL model setup (Fig. 4). This strategy to modify the model's S_r is relatively simple and could similarly be implemented in other land surface models. Moreover, the applied methodology ~~would~~ could allow for a time-varying S_r in LSMs, and hence all four limitations of using sparse root observations mentioned in Sect. 1 could be overcome.

The comparison of the offline simulations with original (CTR) and modified (MD) versions of HTESSEL shows that the difference of the biases in modeled long-term mean climatology of discharge and evaporation fluxes is generally small. On the other hand, the seasonal timing of the discharge flux is significantly improved in MD indicating the beneficial effect of the climate controlled representation of S_r. Consistently, MD improves the correlation with observations for the monthly seasonal climatology of discharge fluxes in 12 out of 15 catchments (with 7 catchments passing 5% significance level) and for the inter-annual monthly discharge anomalies in 14 out of 15 catchments (with 9 catchments passing 5% significance level) (Table S5). Considering the climate region averages, the correlations of monthly seasonal climatology significantly improve in MD compared to CTR from 0.843 to 0.902 (tropical), from 0.741 to 0.855 (temperate) and from 0.860 to 0.951 (Mediterranean). The averaged correlations of the inter-annual monthly anomalies significantly improve in MD compared to CTR from 0.741 to 0.778 (tropical), from 0.795 to 0.847 (temperate) and from 0.705 to 0.785 (Mediterranean). Surprisingly the modeled evaporation is shown to be relatively insensitive to changes in S_r. ~~The apparent insensitivity of evaporation to the changes in model soil depth is probably mainly related to the fact that evaporation~~ In HTESSEL evaporation only depends on the relative moisture content in each soil layer, which in the model is not directly affected by the depth of the soil. Investigation to this insensitivity showed that it is only sensitive during dry periods when evaporation is dominated by transpiration from the fourth layer (Fig. 8). On the other hand, surface and subsurface runoff in HTESSEL depend on the ~~cumulative~~ total moisture content of the soil at any given time. Other than the relative moisture content this depends on the absolute moisture storage capacity of the soil that will vary together with the change in soil depth. Moreover, small changes in absolute fluxes translated to larger relative changes for runoff compared to evaporation (Fig. 6).

As a final conclusion, we believe that a global application of climate controlled root zone parameters has the potential to improve the timing of modeled water fluxes by land surface models, but from the results of this study a significant reduction of annual-mean climatological biases cannot be expected. More work will be needed in the future to improve long-term mean simulation of discharge and evaporation fluxes by exploiting station-based and latest-generation satellite observations. To this aim the use of coordinated multi-model frameworks for the intercomparison of state-of-the-art LSMs could be fundamental.

Code and data availability. Catchment discharge observations were taken from the Australian Bureau of Meteorology and can be downloaded from http://www.bom.gov.au/water/hrs/. FLUXCOM evaporation data were taken from the FLUXCOM initiative and can be downloaded from http://www.fluxcom.org/EF-Download/. Top of the atmosphere radiation data were taken from Mines ParisTech and can be downloaded from http://www.soda-pro.com/web-services/radiation/extraterrestrial-irradiance-and-toa/. The offline HTESSEL model was provided by EC-EARTH, together with the GSWP-3 forcing data, vegetation and soil data. The adapted modules, model output and analysis codes are available upon request. The python scripts used for S_r calculation and statistical significance of the results can be downloaded from https://github.com/fvanoorschot/Python-scripts-van-Oorschot-2021/.

Appendix A: Iterative procedure for transpiration estimation

Daily transpiration is estimated by Eq. (7) with c a coefficient that represents the ratio between transpiration and potential evaporation (Sect. 2.3). With $c = \overline{E_\mathrm{t}}/\overline{E_\mathrm{p}}$ as a constant value, we do not account for inter-annual variability in transpiration caused by the interplay between atmospheric water demand and vegetation-available water supply. Therefore, we add an iterative procedure to estimate annually varying values for c, which is described here.

Steps 1 to 6 describe the procedure used to estimate c with step 1 the initial estimates and step 2 to 6 executed iteratively. i represents the iterations (0–9) and a the hydrological years (1973–2010). P_e, E_t, E_p and S_d are daily values. After ten iterations ($i = 9$) the resulting annual transpiration estimates stabilized and the corresponding storage deficits were used for the Gumbel S_r analysis as described in Sect. 2.3.

1. Initial estimates ($i = 0$) of E_t and S_d with a constant $c_{0,a} = \overline{E}_\mathrm{t}/\overline{E}_\mathrm{p}$ for $a = 1973$–2010.

$$E_{\mathrm{t},0}(t) = c_{0,a}\, E_\mathrm{p}(t) \tag{A1}$$

$$S_{\mathrm{d},0} = \max(0, -\int_{1973}^{2010} (P_\mathrm{e} - E_{\mathrm{t},0})\mathrm{d}t) \tag{A2}$$

2. Calculate the annual change in storage in the root zone (S) with t_0 and t_1 the start and end of a hydrological year.

$$\frac{\mathrm{d}S_{i,a}}{\mathrm{d}t} = S_{\mathrm{d},i}(t_0) - S_{\mathrm{d},i}(t_1) \tag{A3}$$

3. Calculate annual transpiration following the water balance.

$$\overline{E}_{\mathrm{t},a} = \overline{P}_{\mathrm{e},a} - \overline{Q}_a - \frac{\mathrm{d}S_a}{\mathrm{d}t} \tag{A4}$$

4. Calculate c_a for each hydrological year based on the annual E_t estimate from step 3 and calculate daily E_t.

$$c_{i,a} = \frac{\overline{E}_{\mathrm{t},i,a}}{\overline{E}_{\mathrm{p},a}} \tag{A5}$$

480

$$E_{\mathrm{t},i}(t) = c_{i,a} E_\mathrm{p}(t) \tag{A6}$$

5. Calculate storage deficits based on daily E_t from step 4.

$$S_{\mathrm{d},i} = \max(0, -\int_{1973}^{2010} (P_\mathrm{e} - E_{\mathrm{t},i})\mathrm{d}t) \tag{A7}$$

6. The input storage deficit of iteration $i+1$ in step 2 is the average of iteration i and $i-1$

485 $$S_{\mathrm{d},i+1} = \frac{S_{\mathrm{d},i} + S_{\mathrm{d},i-1}}{2} \tag{A8}$$

The following three constraints are set to the iterations:

- The long term water balance closes ($\overline{P}_\mathrm{e} - \overline{Q} - \overline{E}_\mathrm{t} \approx 0$).
- Annual transpiration is always larger than zero and smaller than the annual potential evaporation.
- Variations in c are limited by $c_{0,a} - f\,c_{0,a} < c_{i,a} < c_{0,a} + f\,c_{0,a}$ with f a coefficient set to 0.25.

490 Figure A1 illustrates the iterative approach for storage deficit calculations. Daily P, E_p and E_t based on Eq. (A1) are presented in Fig. A1a. Figure A1b shows annual variations of P_e and E_t. During the years 1980-1984 P_e is clearly less than average and $E_{\mathrm{t},0}$ estimate is likely too high in these years because vegetation has less water available for transpiration this year. The final iteration $E_{\mathrm{t},9}$ provides a more realistic inter-annual pattern of transpiration. Initial and final iteration storage deficits are presented in Fig. A1c.

495 *Author contributions.* The study was conceived by RE and amended with input from all authors. FO carried out the study, analysed the results and wrote the manuscript with input and feedback from RE, MH and AA. Specific knowledge and support for the S_r calculations were provided by MH and specific knowledge and support for the EC-EARTH model were provided by AA.

Competing interests. The authors declare that they have no conflict of interest

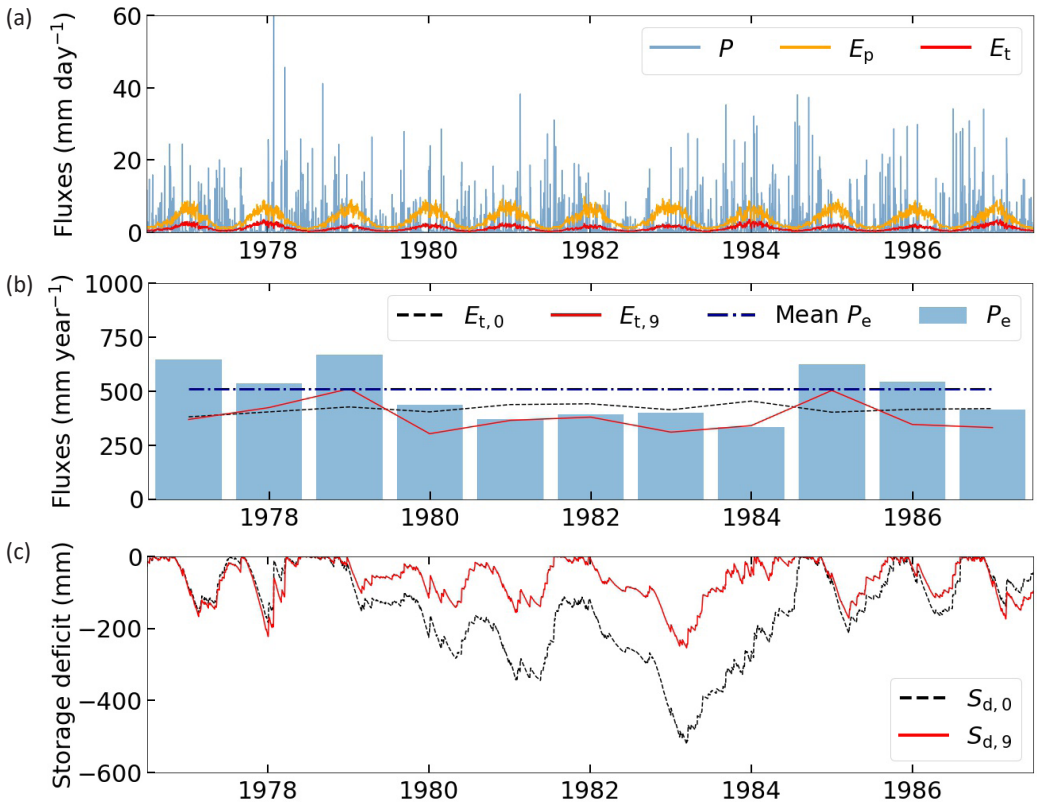

Figure A1. Storage deficit iteration approach in a temperate catchment for the time period 1977–1987. (a) Daily water fluxes with P precipitation, E_p potential evaporation and E_t the initial transpiration calculation based on Eq. (7); (b) Annual water fluxes with P_e effective precipitation, $E_{t,0}$ the initial transpiration estimate and $E_{t,9}$ the final iteration transpiration estimate. Mean P_e is based on the full time period (1973-2010); (c) Daily storage deficit with $S_{d,0}$ the initial calculation and $S_{d,9}$ the final iteration.

Acknowledgements. Acknowledgement is made for the use of ECMWF's computing and archive facilities in this research that were provided by the KNMI and by ECMWF in the framework of special project SPITALES. This work was supported by the European Union's Horizon 2020 research and innovation programme under grant agreement N. 101004156 (CONFESS project). RE acknowledges funding from the Netherlands Organization for Scientific Research (NWO), project number 016.Veni.181.015.

References

Ardilouze, C., Batté, L., Bunzel, F., Decremer, D., Déqué, M., Doblas-Reyes, F. J., Douville, H., Fereday, D., Guemas, V., MacLachlan, C., et al.: Multi-model assessment of the impact of soil moisture initialization on mid-latitude summer predictability, Climate Dynamics, 49, 3959–3974, https://doi.org/10.1007/s00382-017-3555-7, 2017.

Australian Government Bureau of Meteorology: Hydrologic Reference Stations, http://www.bom.gov.au/water/hrs/index.shtml, last access: September 2019, 2019.

Balsamo, G., Viterbo, P., Beijaars, A., van den Hurk, B., Hirschi, M., Betts, A. K., and Scipal, K.: A revised hydrology for the ECMWF model: Verification from field site to terrestrial water storage and impact in the integrated forecast system, Journal of Hydrometeorology, 10, 623–643, https://doi.org/10.1175/2008JHM1068.1, 2009.

Balsamo, G., Pappenberger, F., Dutra, E., Viterbo, P., and van den Hurk, B.: A revised land hydrology in the ECMWF model: a step towards daily water flux prediction in a fully-closed water cycle, Hydrological Processes, 25, 1046–1054, https://doi.org/10.1002/hyp.7808, 2011.

Bouaziz, L., Weerts, A., Schellekens, J., Sprokkereef, E., Stam, J., Savenije, H., and Hrachowitz, M.: Redressing the balance: quantifying net intercatchment groundwater flows, Hydrology and Earth System Sciences, 22, 6415–6434, https://doi.org/10.5194/hess-22-6415-2018, 2018.

Canadell, J., Jackson, R., Ehleringer, J., Mooney, H., Sala, O., and Schulze, E.-D.: Maximum rooting depth of vegetation types at the global scale, Oecologia, 108, 583–595, https://doi.org/10.1007/BF00329030, 1996.

Collins, D. B. and Bras, R. L.: Plant rooting strategies in water-limited ecosystems, Water Resources Research, 43, 1–10, https://doi.org/10.1029/2006WR005541, 2007.

Condon, L. E., Markovich, K. H., Kelleher, C. A., McDonnell, J. J., Ferguson, G., and McIntosh, J. C.: Where Is the Bottom of a Watershed?, Water Resources Research, 56, e2019WR026 010, https://doi.org/10.1029/2019WR026010, 2020.

De Boer-Euser, T., McMillan, H. K., Hrachowitz, M., Winsemius, H. C., and Savenije, H. H.: Influence of soil and climate on root zone storage capacity, Water Resources Research, 52, 2009–2024, https://doi.org/10.1002/2015WR018115, 2016.

de Rosnay, P. and Polcher, J.: Modelling root water uptake in a complex land surface scheme coupled to a GCM, Hydrology and Earth System Sciences, 2, 239–255, https://doi.org/10.5194/hess-2-239-1998, 1998.

Desborough, C. E.: The impact of root weighting on the response of transpiration to moisture stress in land surface schemes, Monthly Weather Review, 125, 1920–1930, https://doi.org/10.1175/1520-0493(1997)125<1920:TIORWO>2.0.CO;2, 1997.

Dümenil, L. and Todini, E.: A rainfall–runoff scheme for use in the Hamburg climate model, in: Advances in Theoretical Hydrology, edited by O'Kane, J. P., European Geophysical Society Series on Hydrological Sciences, pp. 129–157, Elsevier, Amsterdam, https://doi.org/10.1016/B978-0-444-89831-9.50016-8, 1992.

ECMWF: Part IV: Physical Processes, IFS Documentation, https://www.ecmwf.int/node/17117, 2016.

Euser, T., Hrachowitz, M., Winsemius, H. C., and Savenije, H. H.: The effect of forcing and landscape distribution on performance and consistency of model structures, Hydrological Processes, 29, 3727–3743, https://doi.org/10.1002/hyp.10445, 2015.

FAO: Digital Soil Map of the World (DSMW), Tech. rep., Food and Agricultural Organization of the United Nations, re-issued version, 2003.

Feddes, R. A., Hoff, H., Bruen, M., Dawson, T., De Rosnay, P., Dirmeyer, P., Jackson, R. B., Kabat, P., Kleidon, A., Lilly, A., and Pitman, A. J.: Modeling root water uptake in hydrological and climate models, Bulletin of the American Meteorological Society, 82, 2797–2809, https://doi.org/10.1175/1520-0477(2001)082<2797:MRWUIH>2.3.CO;2, 2001.

Ferguson, I. M., Jefferson, J. L., Maxwell, R. M., and Kollet, S. J.: Effects of root water uptake formulation on simulated water and energy budgets at local and basin scales, Environmental Earth Sciences, 75, 1–15, https://doi.org/10.1007/s12665-015-5041-z, 2016.

Gao, H., Hrachowitz, M., Schymanski, S. J., Fenicia, F., Sriwongsitanon, N., and Savenije, H. H. G.: Climate controls how ecosystems size the root zone storage capacity at catchment scale, Geophysical Research Letters, 41, 7916–7923, https://doi.org/10.1002/2014GL061668, 2014.

Gentine, P., D'Odorico, P., Lintner, B. R., Sivandran, G., and Salvucci, G.: Interdependence of climate, soil, and vegetation as constrained by the Budyko curve, Geophysical Research Letters, 39, 2–7, https://doi.org/10.1029/2012GL053492, 2012.

Gerrits, A. M., Pfister, L., and Savenije, H. H.: Spatial and temporal variability of canopy and forest floor interception in a beech forest, Hydrological Processes, 24, 3011–3025, https://doi.org/10.1002/hyp.7712, 2010.

Gharari, S., Clark, M. P., Mizukami, N., Wong, J. S., Pietroniro, A., and Wheater, H. S.: Improving the Representation of Subsurface Water Movement in Land Models, Journal of Hydrometeorology, 20, 2401 – 2418, https://doi.org/10.1175/JHM-D-19-0108.1, 2019.

Gumbel, E. J.: Les valeurs extrêmes des distributions statistiques, Annales de l'institut Henri Poincaré, 5, 115–158, 1935.

Guswa, A. J.: The influence of climate on root depth: A carbon cost-benefit analysis, Water Resources Research, 44, 1–11, https://doi.org/10.1029/2007WR006384, 2008.

Hagemann, S. and Stacke, T.: Impact of the soil hydrology scheme on simulated soil moisture memory, Climate Dynamics, 44, 1731–1750, https://doi.org/10.1007/s00382-014-2221-6, 2015.

Hargreaves, G. H. and Samani, Z. A.: Estimating potential evapotranspiration, Journal of the irrigation and Drainage Division, 108, 225–230, 1982.

Herwitz, S. R.: Interception storage capacities of tropical rainforest canopy trees, Journal of Hydrology, 77, 237–252, https://doi.org/10.1016/0022-1694(85)90209-4, 1985.

Hrachowitz, M., Stockinger, M., Coenders-Gerrits, M., van der Ent, R., Bogena, H., Lücke, A., and Stumpp, C.: Deforestation reduces the vegetation-accessible water storage in the unsaturated soil and affects catchment travel time distributions and young water fractions, Hydrology and Earth System Sciences Discussions, 2020, 1–43, https://doi.org/10.5194/hess-2020-293, 2020.

Jackson, R. B., Canadell, J., Ehleringer, J. R., Mooney, H. A., Sala, O. E., and Schulze, E. D.: A global analysis of root distributions for terrestrial biomes, Oecologia, 108, 389–411, https://doi.org/10.1007/BF00333714, 1996.

Jeffrey, S. J., Carter, J. O., Moodie, K. B., and Beswick, A. R.: Using spatial interpolation to construct a comprehensive archive of Australian climate data, Environmental Modelling and Software, 16, 309 – 330, https://doi.org/https://doi.org/10.1016/S1364-8152(01)00008-1, 2001.

Jung, M., Koirala, S., Weber, U., Ichii, K., Gans, F., Camps-Valls, G., Papale, D., Schwalm, C., Tramontana, G., and Reichstein, M.: The FLUXCOM ensemble of global land-atmosphere energy fluxes, Scientific data, 6, 74, https://doi.org/10.1038/s41597-019-0076-8, 2019.

Kim, H.: Global Soil Wetness Project Phase 3 Atmospheric Boundary Conditions (Experiment 1) [Data set], Data Integration and Analysis System (DIAS), https://doi.org/10.20783/DIAS.501, 2017.

Kleidon, A.: Global datasets of rooting zone depth inferred from inverse methods, Journal of Climate, 17, 2714–2722, https://doi.org/10.1175/1520-0442(2004)017<2714:GDORZD>2.0.CO;2, 2004.

Kleidon, A. and Heimann, M.: A method of determining rooting depth from a terrestrial biosphere model and its impacts on the global water and carbon cycle, Global Change Biology, 4, 275–286, https://doi.org/10.1046/j.1365-2486.1998.00152.x, 1998.

Ma, N., Szilagyi, J., and Jozsa, J.: Benchmarking large-scale evapotranspiration estimates: A perspective from a calibration-free complementary relationship approach and FLUXCOM, Journal of Hydrology, 590, https://doi.org/10.1016/j.jhydrol.2020.125221, 2020.

Mahfouf, J. F., Ciret, C., Ducharne, A., Irannejad, P., Noilhan, J., Shao, Y., Thornton, P., Xue, Y., and Yang, Z. L.: Analysis of transpiration results from the RICE and PILPS workshop, Global and Planetary Change, 13, 73–88, https://doi.org/10.1016/0921-8181(95)00039-9, 1996.

Milly, P. C.: Climate, soil water storage, and the average annual water balance, Water Resources Research, 30, 2143–2156, https://doi.org/10.1029/94WR00586, 1994.

Mines ParisTech Solar radiation Data: Extraterrestrial irradiance (e0) and top of atmosphere (toa) radiation, http://www.soda-pro.com/web-services/radiation/extraterrestrial-irradiance-and-toa, last access: September 2019, 2016.

Nijzink, R., Hutton, C., Pechlivanidis, I., Capell, R., Arheimer, B., Freer, J., Han, D., Wagener, T., McGuire, K., Savenije, H., and Hrachowitz, M.: The evolution of root-zone moisture capacities after deforestation: a step towards hydrological predictions under change?, Hydrology and Earth System Sciences, 20, 4775–4799, https://doi.org/10.5194/hess-20-4775-2016, 2016.

Norby, R. and Jackson, R.: Root dynamics and global change: seeking an ecosystem perspective, New Phytologist, 147, 1–2, https://doi.org/10.1046/j.1469-8137.2000.00674.x, 2000.

Oudin, L., Andréassian, V., Perrin, C., and Anctil, F.: Locating the sources of low-pass behavior within rainfall-runoff models, Water Resources Research, 40, https://doi.org/10.1029/2004WR003291, 2004.

Pan, S., Pan, N., Tian, H., Friedlingstein, P., Sitch, S., Shi, H., Arora, V. K., Haverd, V., Jain, A. K., Kato, E., Lienert, S., Lombardozzi, D., Ottle, C., Poulter, B., and Zaehle, S.: Evaluation of global terrestrial evapotranspiration by state-of-the-art approaches in remote sensing, machine learning, and land surface models, Hydrology and Earth System Sciences, 24, 1485–1509, https://doi.org/10.5194/hess-2019-409, 2020.

Pastorello, G., Trotta, C., Canfora, E., et al.: The FLUXNET2015 dataset and the ONEFlux processing pipeline for eddy covariance data, Scientific Data, 7, 225, https://doi.org/10.1038/s41597-020-0534-3, 2020.

Pitman, A. J.: The evolution of, and revolution in, land surface schemes designed for climate models, International Journal of Climatology, 23, 479–510, https://doi.org/10.1002/joc.893, 2003.

Sakschewski, B., von Bloh, W., Drüke, M., Sörensson, A., Ruscica, R., Langerwisch, F., Billing, M., Bereswill, S., Hirota, M., Oliveira, R., Heinke, J., and Thonicke, K.: Variable tree rooting strategies improve tropical productivity and evapotranspiration in a dynamic global vegetation model, Biogeosciences Discussions, pp. 1–35, https://doi.org/10.5194/bg-2020-97, 2020.

Schenk, H. J. and Jackson, R. B.: Rooting depths, lateral root spreads and below-ground/above-ground allometries of plants in water-limited ecosystems, Journal of Ecology, 90, 480–494, https://doi.org/10.1046/j.1365-2745.2002.00682.x, 2002a.

Schenk, H. J. and Jackson, R. B.: The Global Biogeography of Roots, Ecological Monographs, 72, 311–328, https://doi.org/10.1890/0012-9615(2002)072[0311:TGBOR]2.0.CO;2, 2002b.

Schlesinger, W. H. and Jasechko, S.: Transpiration in the global water cycle, Agricultural and Forest Meteorology, 189-190, 115 – 117, https://doi.org/10.1016/j.agrformet.2014.01.011, 2014.

Seneviratne, S. I., Koster, R. D., Guo, Z., Dirmeyer, P. A., Kowalczyk, E., Lawrence, D., Liu, P., Lu, C. H., Mocko, D., Oleson, K. W., and Verseghy, D.: Soil moisture memory in AGCM simulations: Analysis of global land-atmosphere coupling experiment (GLACE) data, Journal of Hydrometeorology, 7, 1090–1112, https://doi.org/10.1175/JHM533.1, 2006.

Seneviratne, S. I., Corti, T., Davin, E. L., Hirschi, M., Jaeger, E. B., Lehner, I., Orlowsky, B., and Teuling, A. J.: Investigating soil moisture-climate interactions in a changing climate: A review, Earth-Science Reviews, 99, 125–161, https://doi.org/10.1016/j.earscirev.2010.02.004, 2010.

Singh, C., Wang-Erlandsson, L., Fetzer, I., Rockström, J., and van der Ent, R.: Rootzone storage capacity reveals drought coping strategies along rainforest-savanna transitions, Environmental Research Letters, 15, 124 021, https://doi.org/10.1088/1748-9326/abc377, 2020.

Sivandran, G. and Bras, R. L.: Dynamic root distributions in ecohydrological modeling: A case study at Walnut Gulch Experimental Watershed, Water Resources Research, 49, 3292–3305, https://doi.org/10.1002/wrcr.20245, 2013.

Teuling, A. J., Seneviratne, S. I., Williams, C., and Troch, P. A.: Observed timescales of evapotranspiration response to soil moisture, Geophysical Research Letters, 33, https://doi.org/10.1029/2006GL028178, 2006.

van den Hurk, B. and Viterbo, P.: The Torne-Kalix PILPS 2 (e) experiment as a test bed for modifications to the ECMWF land surface scheme, Global and Planetary Change, 38, 165–173, 2003.

van den Hurk, B., Viterbo, P., Beljaars, A., and Betts, A.: Offline validation of the ERA40 surface scheme, https://doi.org/10.21957/9aoaspz8, 2000.

van den Hurk, B., Kim, H., Krinner, G., Seneviratne, S. I., Derksen, C., Oki, T., Douville, H., Colin, J., Ducharne, A., Cheruy, F., Viovy, N., Puma, M. J., Wada, Y., Li, W., Jia, B., Alessandri, A., Lawrence, D. M., Weedon, G. P., Ellis, R., Hagemann, S., Mao, J., Flanner, M. G., Zampieri, M., Materia, S., Law, R. M., and Sheffield, J.: LS3MIP (v1.0) contribution to CMIP6: the Land Surface, Snow and Soil moisture Model Intercomparison Project – aims, setup and expected outcome, Geoscientific Model Development, 9, 2809–2832, https://doi.org/10.5194/gmd-9-2809-2016, 2016.

Van Genuchten, M. T.: A closed-form equation for predicting the hydraulic conductivity of unsaturated soils 1, Soil science society of America journal, 44, 892–898, https://doi.org/10.2136/sssaj1980.03615995004400050002x, 1980.

Wang-Erlandsson, L., Bastiaanssen, W. G., Gao, H., Jagermeyr, J., Senay, G. B., Van Dijk, A. I., Guerschman, J. P., Keys, P. W., Gordon, L. J., and Savenije, H. H.: Global root zone storage capacity from satellite-based evaporation, Hydrology and Earth System Sciences, 20, 1459–1481, https://doi.org/10.5194/hess-20-1459-2016, 2016.

Wartenburger, R., Seneviratne, S. I., Hirschi, M., Chang, J., Ciais, P., Deryng, D., Elliott, J., Folberth, C., Gosling, S. N., Gudmundsson, L., Henrot, A.-J., Hickler, T., Ito, A., Khabarov, N., Kim, H., Leng, G., Liu, J., Liu, X., Masaki, Y., Morfopoulos, C., Müller, C., Schmied, H. M., Nishina, K., Orth, R., Pokhrel, Y., Pugh, T. A. M., Satoh, Y., Schaphoff, S., Schmid, E., Sheffield, J., Stacke, T., Steinkamp, J., Tang, Q., Thiery, W., Wada, Y., Wang, X., Weedon, G. P., Yang, H., and Zhou, T.: Evapotranspiration simulations in ISIMIP2a—Evaluation of spatio-temporal characteristics with a comprehensive ensemble of independent datasets, Environmental Research Letters, 13, 075 001, https://doi.org/10.1088/1748-9326/aac4bb, 2018.

Zeng, X., Dai, Y. J., Dickinson, R. E., and Shaikh, M.: The role of root distribution for climate simulation over land, Geophysical Research Letters, 25, 4533–4536, https://doi.org/10.1029/1998GL900216, 1998.